



HAL
open science

Structural, dielectric, and ferroelectric properties of Na-0.5(Bi_{1-x}Nd_x)(0.5)TiO₃ ceramics for energy storage and electrocaloric applications

Manal Benyoussef, Moneim Zannen, Jamal Belhadi, Bouchaib Manoun, Zdravko Kutnjak, Damjan Vengust, Matjaz Spreitzer, Mimoun El Marssi, Abdelilah Lahmar

► To cite this version:

Manal Benyoussef, Moneim Zannen, Jamal Belhadi, Bouchaib Manoun, Zdravko Kutnjak, et al.. Structural, dielectric, and ferroelectric properties of Na-0.5(Bi_{1-x}Nd_x)(0.5)TiO₃ ceramics for energy storage and electrocaloric applications. *Ceramics International*, 2021, 47 (18), pp.26539-26551. 10.1016/j.ceramint.2021.06.068 . hal-03608402

HAL Id: hal-03608402

<https://u-picardie.hal.science/hal-03608402>

Submitted on 2 Aug 2023

HAL is a multi-disciplinary open access archive for the deposit and dissemination of scientific research documents, whether they are published or not. The documents may come from teaching and research institutions in France or abroad, or from public or private research centers.

L'archive ouverte pluridisciplinaire **HAL**, est destinée au dépôt et à la diffusion de documents scientifiques de niveau recherche, publiés ou non, émanant des établissements d'enseignement et de recherche français ou étrangers, des laboratoires publics ou privés.



Distributed under a Creative Commons Attribution - NonCommercial 4.0 International License

Structural, dielectric, and ferroelectric properties of $\text{Na}_{0.5}(\text{Bi}_{1-x}\text{Nd}_x)_{0.5}\text{TiO}_3$ ceramics for energy storage and electrocaloric applications

Manal Benyoussef ^{a,*}, Moneim Zannen ^{b,*}, Jamal Belhadi ^c, Bouchaib Manoun ^d, Zdravko Kutnjak ^e, Damjan Vengust ^c, Matjaz Spreitzer ^c, Mimoun El Marssi ^a, Abdelilah Lahmar ^a

^a Laboratory of Physics of Condensed Matter (LPMC), University of Picardie Jules Verne, Scientific Pole, 33 rue Saint-Leu, 80039, Amiens Cedex 1, France.

^b Laboratory of Interfaces and Advanced Materials (LIMA), Faculty of Sciences of Monastir, University of Monastir, Bd. Of the Environment, Monastir, 5019, Tunisia.

^c Department of Advanced Materials, Jozef Stefan Institute, Ljubljana, Slovenia.

^d Université Hassan 1^{er}, Laboratoire des Sciences des Matériaux, des Milieux et de la Modélisation (LS3M), 25000, Khouribga, Morocco.

^e Department of Condensed Matter Physics, Jozef Stefan Institute, Ljubljana, Slovenia.

Abstract

Lead-free relaxor ferroelectric $\text{Na}_{0.5}(\text{Bi}_{1-x}\text{Nd}_x)_{0.5}\text{TiO}_3$ ($x\text{NdNBT}$, $x = 0 - 30\%$) ceramics were synthesized using the conventional solid-state method. Detailed Rietveld refinement revealed transitions from rhombohedral ($x = 0, 5\%$), to a coexistence of $R3c$ and $Pnma$ symmetries ($x = 10, 15\%$), followed by a tetragonal $P4/mmm$ phase for the high Nd-concentrations ($x = 25, 30\%$). High-temperature dielectric stability was found over a large temperature range (for instance $\pm 15\%$ from -90°C to 405°C for $x = 30\%$) with very low dielectric losses, especially at high temperatures. The substitution of Bi^{3+} by Nd^{3+} results in a perturbation of the ferroelectric order and favors short-range polar regions in the system. From the ferroelectric measurements, we demonstrated the stabilization of a coexistence of non-ergodic and ergodic relaxor state or ergodic relaxor state at specific doping concentrations. Besides, high-energy storage properties were obtained at high temperatures, with $W_{\text{rec}} > 1.15 \text{ J/cm}^3$ in the temperature range $140^\circ\text{C} - 200^\circ\text{C}$ for the 5NdNBT and a moderate W_{rec} between 0.5 and 0.77 J/cm^3 in a large temperature range from 25°C to 200°C and with high efficiency $> 70\%$ for 10NdNBT composition. In addition, a high electrocaloric response ($\Delta T = 1.8 \text{ K}$ at 95 kV/cm) was found using the indirect method for the 5NdNBT composition, with great temperature stability below 20% over a broad temperature range ($80 - 140^\circ\text{C}$) and with a high $\Delta T/\Delta E > 0.19 \text{ K m/V}$. The obtained electrocaloric response was related to the thermal evolution of the polar regions in mixed ergodic and non-ergodic relaxor states under an applied electric field.

Corresponding author: manal.benyoussef@u-picardie.fr (M. Benyoussef)
moneimchimie2006@yahoo.fr (M. Zannen)

Keywords: $\text{Na}_{0.5}(\text{Bi}_{1-x}\text{Nd}_x)_{0.5}\text{TiO}_3$ ceramics; NER/ER relaxor states; dielectric properties; energy storage; electrocaloric effect.

1. Introduction

First discovered by Smolensky *et al.* in lead magnesium niobate [1], relaxor ferroelectric (RF) materials have seen an increasing growth over the past years owing to their outstanding dielectric and electrochemical properties [2,3]. The valuable properties of relaxors are principally related to their distinct polar structure, i.e., the existence of polar nanoregions (PNRs), and their ability to respond to an external electric field [4,5]. It is believed that relaxor features are mainly driven by chemical disorder in the A/B-site mixed perovskites [6]. The former chemical disorder is assumed to induce local random fields, which are responsible for the presence of polar nanoregions (PNRs). In contrast to FEs, the presence of PNRs in RFs and their specific switching under an applied electric field makes these materials very attractive for energy storage applications and cooling devices that can operate in a wide temperature range. Non-ergodic relaxors (NER) in their induced ferroelectric state, with a correspondingly high remanent polarization and coercive field, have limited energy storage performances. In contrast, ergodic relaxors (ER), which can reversibly be switched from short-range polar order to long-range ferroelectric polar order under an applied electric field, exhibit low remanent polarization and coercive field. Such properties are very advantageous to energy storage performances. Interestingly, through chemical modification into a specific system, the initial non-ergodic relaxor state can either transform to a complete ergodic relaxor state, or induce a coexistence of both NER and ER relaxor states in the unpoled state [7–9]. Consequently, chemically tailored systems with induced NER and ER relaxor states have emerged as an alternative to FEs owing to their excellent energy storage and electrocaloric effect (ECE) properties in a wide temperature range owing to their diffuse phase transition [10].

Due to their outstanding piezoelectric, electromechanical, electrocaloric, and energy storage performances, the lead-based RFs, such as $\text{Pb}(\text{Mg}_{1/3}\text{Nb}_{2/3})\text{O}_3\text{--PbTiO}_3$, $\text{PbZn}_{1/3}\text{Nb}_{2/3}\text{O}_3$, and $\text{PbSc}_{1/2}\text{Nb}_{1/2}\text{O}_3$ based materials were considered and much studied initially in both bulk and thin-film form [11–15]. However, due to environmental concerns, the European Parliament imposed restrictions on some hazardous elements such as lead (Pb), in the electrical and electronic equipment (2011/65/Eu (RoHS)) [16]. Therefore, during the last decades, there has been considerable interest in the development of lead-free FE and RF materials, and various materials have been considered to replace lead-based toxic systems [17–29]. The lead-free $\text{Na}_{0.5}\text{Bi}_{0.5}\text{TiO}_3$ (NBT) based ceramics are regarded as one of the most promising RF materials thanks to their particular and exciting structural and dielectric features. The pure NBT composition presents a non-ergodic relaxor state below the depolarization temperature (T_d) [30,31]. It is among the rare A-site mixed perovskites since the majority of the studied relaxor systems are of B-site mixed perovskites [32]. In addition, NBT exhibits high spontaneous polarization of $38 \mu\text{C}/\text{cm}^2$, due to the lone pair effect of Bi^{3+} , similar to that of the Pb^{2+} element. Besides, the strong hybridization of bismuth $6s^2$ and oxygen $2p$ orbitals leads to Bi^{3+} off-centering, thence driving ferroelectricity within the system [33]. Of particular interest, the multiple dielectric anomalies of the NBT as well as its exciting relaxor properties make the system very advantageous for numerous applications. Despite its high potential, the Achilles' heel of the non-ergodic relaxor NBT system, is its high conductivity which limits its integration in devices [34–37].

As a result, the NBT system was stormed by diverse research groups to improve its physical properties through chemical tailoring. Within this scope, promising binary/ternary systems were developed for piezoelectric, energy storage, and electrocaloric applications, among which one can find $\text{Na}_{0.5}\text{Bi}_{0.5}\text{TiO}_3\text{-BaTiO}_3$, $\text{Na}_{0.5}\text{Bi}_{0.5}\text{TiO}_3\text{-K}_{0.5}\text{Bi}_{0.5}\text{TiO}_3$, $\text{Na}_{0.5}\text{Bi}_{0.5}\text{TiO}_3\text{-NaNbO}_3$, $\text{Na}_{0.5}\text{Bi}_{0.5}\text{TiO}_3\text{-BaTiO}_3\text{-K}_{0.5}\text{Na}_{0.5}\text{NbO}_3$, and $\text{Na}_{0.5}\text{Bi}_{0.5}\text{TiO}_3\text{-SrTiO}_3$ systems [38–42,27–29]. Further, using specific doping elements on such systems, the energy storage properties can be enhanced. Recently, Guo et al. reported high energy storage performances on ZrO_2 doped NBT-ST ceramics reaching $W_{\text{rec}} = 2.83 \text{ J/cm}^3$ ($\eta = 83.9\%$) at 220 kV/cm [28]. Using SnO_2 doping on NBT-ST ceramics, Zhang et al. reported an energy density of 2.35 J/cm^3 at 180 kV/cm [27].

On the other hand, doping with rare-earth elements is considered an elegant way to control and improve the physical properties of the NBT system [43–46]. Rare earth introduction can result in a change in the ordering degree of the A/B-site cations, and induce local random fields/bonds within the system [47–49]. Therefore, giving rise to local structural heterogeneities, which are essential in the view of improving the physical properties of materials. Recently, Deng *et al.* reported on an enhanced piezoelectric response in samarium doped $\text{Bi}_{0.5}(\text{Na}_{0.8}\text{K}_{0.2})_{0.5}\text{TiO}_3$ ceramics [50]. Rare-earth doping was also reported to significantly improve the piezoelectric properties in the relaxor ferroelectric PMN-PT ceramics/single crystals due to the induced nanoscale structural heterogeneities [51].

Within this scope, in the present work, we will highlight the effect of neodymium (Nd^{3+}) doping on the structural, dielectric, energy storage, and electrocaloric properties of $\text{Na}_{0.5}(\text{Bi}_{1-x}\text{Nd}_x)_{0.5}\text{TiO}_3$ ($x\text{NdNBT}$) ceramics with ($0 \leq x \leq 30\%$). The substitution of Bi^{3+} by Nd^{3+} in the A-site of the ABO_3 perovskite induced local structural heterogeneities and reduced the long-range polar ordering leading to a change in the structural and electrical properties. By using a specific level of Nd^{3+} doping, both ER with PNRs or coexistence of both ER and NER relaxor states could be stabilized. The recoverable energy storage density and ECE and their thermal stability were investigated. The obtained results show that rare earth doping in NBT based ceramics could be an alternative way to tailor the dielectric and ferroelectric properties. Besides, it can produce high and stable energy storage and ECE response over a wide temperature range.

2. Methods

Conventional solid-state method was used to elaborate $\text{Na}_{0.5}(\text{Bi}_{1-x}\text{Nd}_x)_{0.5}\text{TiO}_3$ ($x\text{NdNBT}$) solid solutions with various concentrations ($x = 0 - 30\%$). Stoichiometric amounts of Na_2CO_3 (99.997%), Bi_2O_3 (99.975%), TiO_2 (99.9%), and Nd_2O_3 (99.99%) powders were thoroughly ball milled at 180 rpm for 4h using yttria-stabilized zirconia balls in ethanol media. The obtained milled powders were then dried, uniaxially pressed into pellets, and placed into a tube furnace for calcination at $800^\circ\text{C}/3\text{h}$. After the calcination process, the pellets were crushed and grounded in an agate mortar. Thence, the powders were again milled at 180 rpm for 4h. The granulometric analysis was used with a laser granulometry (Cilas 850, Marcousis) showed that the median size of the resulted particles was less than $1 \mu\text{m}$. The finely milled powders were uniaxially pressed into pellet, and then cold isostatically pressed at 750 MPa. Finally, the pressed pellets were sintered between 1100°C and $1130^\circ\text{C}/3\text{h}$ in an air

atmosphere with a cooling/heating rate of 5°C/min. The density of the pellet was measured using Archimedes' methods taking ethanol as the immersion fluid, and high-density values were obtained (> 95%). Room-temperature X-ray powder diffraction patterns were recorded on a discover Bruker diffractometer (CuK α = 1.5406 Å), with a step scan increment of 0.01313° in the 2 θ range (20-90°). The indexation of X-ray powder diffraction patterns for our compounds was performed by means of the computer program Dicvol. Scanning electron microscope (SEM; Environmental Quanta 200 FEG, FEI) was used to extract information about the microstructure of our samples. The Raman spectra were recorded at room temperature using a micro-Raman Renishaw spectrometer equipped with a CCD detector. The red laser was used to excite the samples (633 nm). The dielectric measurements were carried out using a Solartron Impedance analyzer SI-12060. Ferroelectric hysteresis loops were collected at 1Hz at different temperatures using a ferroelectric test system (TF Analyzer 2000, aix-ACCT).

3. Results and discussion

3.1. Structural and microstructural analysis

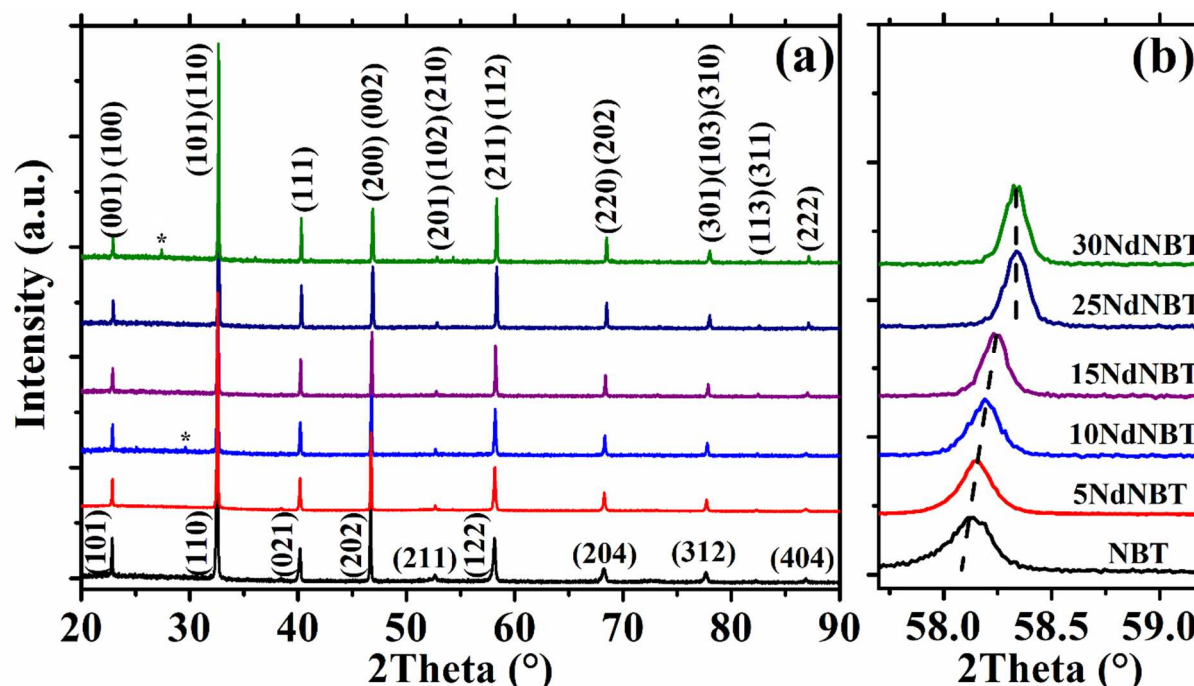


Fig. 1: Room temperature X-ray diffraction patterns of xNdNBT sintered ceramics: (a) $x = 0 - 30\%$. (b): magnified (122) peak of the ceramics.

The X-ray powder diffraction (XRD) patterns at room temperature of the series $\text{Na}_{0.5}(\text{Bi}_{1-x}\text{Nd}_x)_{0.5}\text{TiO}_3$ (named xNdNBT, $x = 0 - 30\%$) compounds are shown in Fig. 1(a). The X-ray diffraction profiles of xNdNBT highlight the formation of a perovskite structure. However, low-intensity impurities were observed around 25-30°. To give an insight into the phase structure evolution of xNdNBT system, a locally magnified (122) peak of the ceramics is presented in Fig. 1(b). The shift to high angles suggests that Bi was well substituted by Nd to form xNdNBT ceramics. Notice that for $x = 30\%$, no shift was observed, which might speak

for a symmetry change at $x = 25\%$. Detailed structural refinements were performed to highlight the structural change.

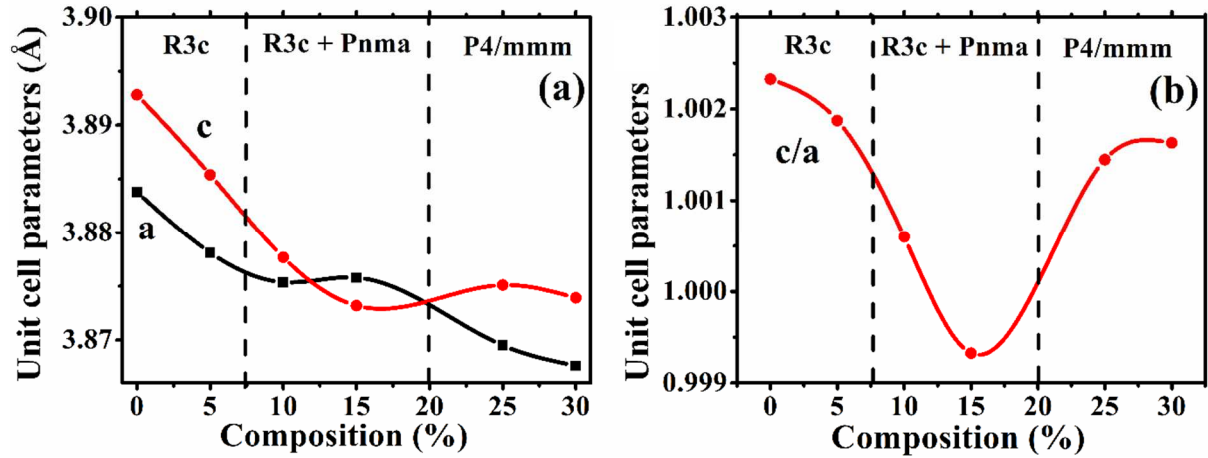


Fig. 2: (a) The variations of the equivalents lattice parameters and, (b) the c/a ratio in the studied compositions of the perovskite series $x\text{NdNBT}$, $x = 0 - 30\%$, as a function of Nd^{3+} amount.

Table S1 gathers the refined unit cell parameters of $x\text{NdNBT}$ compositions ($x = 0 - 30\%$). Interestingly, during the refinements, different types of structures were identified depending on the composition. In the compositional range of $0 \leq x \leq 5\%$, the structure crystallizes in a rhombohedral symmetry ($R3c$), isostructural to the pure NBT system. Besides, a mixture of rhombohedral symmetry ($R3c$) and an orthorhombic phase ($Pnma$) was observed for the $10 \leq x \leq 15\%$ range. For the highest doping composition labeled as 25NdNBT and 30NdNBT, the structure is found to be tetragonal with a $P4/mmm$ space group.

To represent and evaluate the unit cell parameters, we used equivalent pseudocubic unit cell parameters (Fig. 2(a, b)). Besides, to not clutter the illustration, we only present the predominant rhombohedral parameters for the compositions with mixed phases ($x = 10\%$, 15%). From Fig. 2 we can see that as Nd doping increases to 15%, the unit cell parameters as well as c/a ratio decreases, owing to the substitution of larger A-site cations ($r_{\text{Bi}^{3+}} = 1.17 \text{ \AA}$) by smaller ones ($r_{\text{Nd}^{3+}} = 1.109 \text{ \AA}$). With further incorporation of Nd in the A site, a sudden change of the slope (c/a) was observed leading to a significant increase of the unit cell parameters. This evolution is directly related to the structural phase transition to the tetragonal ($P4/mmm$) phase. For the highest doping compositions, the transition to the non-polar tetragonal phase can be explained by the substitution of the stereochemically active lone pair ion by neodymium ion, which induces a decline of the stereochemical activity of Bi-O bonds [52]. Fig. 3(a-c) present the fitted x-ray diffraction patterns of the rhombohedral 5NdNBT, rhombohedral + orthorhombic 15NdNBT, and tetragonal 25NdNBT ceramics. In the structural model of the rhombohedral system ($R3c$) $\text{Na}^{2+}/\text{Bi}^{3+}/\text{Nd}^{3+}$ and Ti^{4+} are placed at the 6a (0, 0, z) sites; the oxygen atoms occupy the 18b (x, y, z) sites. In the structural model of the tetragonal system ($P4/mmm$) $\text{Na}^{2+}/\text{Bi}^{3+}/\text{Nd}^{3+}$ and Ti^{4+} are placed at the sites 1a (0, 0, 0) and 1d ($1/2, 1/2, 1/2$), respectively; the oxygen atoms occupy two positions: the sites 1c ($1/2, 1/2, 0$) and 2e ($1/2, 0, 1/2$).

Schematic views of the crystal structures for 5NdNBT with the $R3c$ space group and 25NdNBT with $P4/mmm$ space group are presented in the insets of Fig. 3. The quality of

structural refinements was examined through the goodness of the R_F , R_B , R_P , R_{WP} , and R_{exp} reliability factors. The crystallographic details of the Rietveld refinement parameters of the compositions 5NdNBT, and 25NdNBT are listed in Table S2. The atomic positions, occupancy, and isotropic atomic displacement parameters of the perovskite series for $\text{Na}_{0.5}(\text{Bi}_{1-x}\text{Nd}_x)_{0.5}\text{TiO}_3$ are summarized in Table S3.

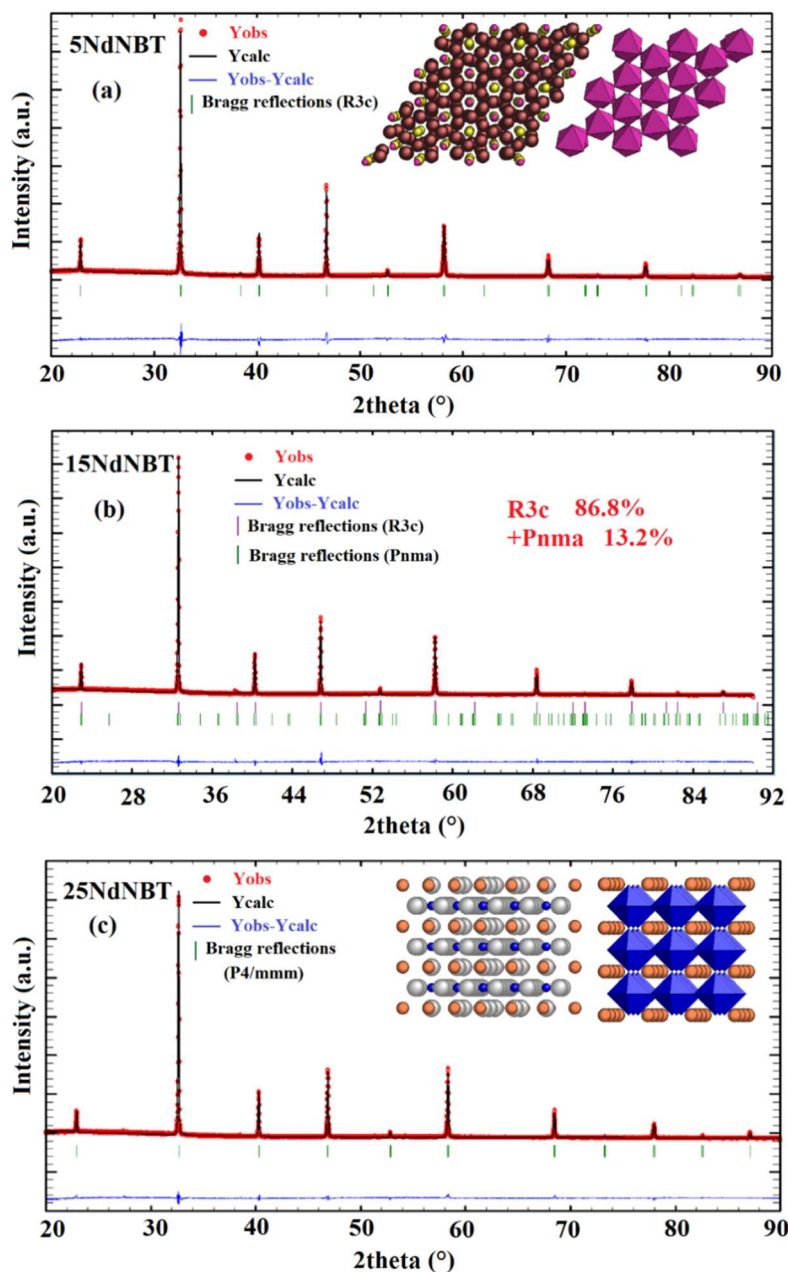


Fig. 3: Final Rietveld refinement plots of X-ray diffraction patterns for (a) 5NdNBT, (b) 15NdNBT, and (c) 25NdNBT: observed, calculated, and their difference. The calculated positions of Bragg reflections are marked by vertical markers. Insets show different structural views of the rhombohedral and tetragonal phases. For 5NdNBT, yellow spheres: Na/Bi/Nd cations, pink spheres: Ti cations, brown spheres: O anions, pink polyhedra: TiO_6 octahedra. For 25NdNBT, orange spheres: Na/Bi/Nd cations, blue spheres: Ti cations, grey spheres: O anions, blue polyhedra: TiO_6 octahedra.

From the analysis of the various inter-atomic distances (Table S4), Na/Bi/Nd cations are surrounded by 12 oxygen atoms, which form (Na/Bi/Nd) O_{12} polyhedra with oxygen anions. The Na/Bi/Nd-O bond lengths vary from 2.55 to 2.95 Å for 5NdNBT showing a significant distortion. For 25NdNBT, these distances vary from 2.736 to 2.738 Å showing a regular polyhedron. It is also observed that Ti^{4+} cations at the B-sites form with the oxygen atoms TiO_6 octahedra as shown in the insets of Fig. 3. These octahedra are connected by oxygen atoms to create a three-dimensional network. The TiO_6 octahedra are only distorted in the $R3c$ space group (Ti-O distances vary from 1.85 to 2.06 Å). The octahedral rotation induced by increasing doping of Nd^{3+} transforms the non-centrosymmetric rhombohedral ($R3c$) structure to the centrosymmetric tetragonal ($P4/mmm$) structure for $x = 25\%$ and 30% (Ti-O distances vary from 1.935 to 1.938 Å).

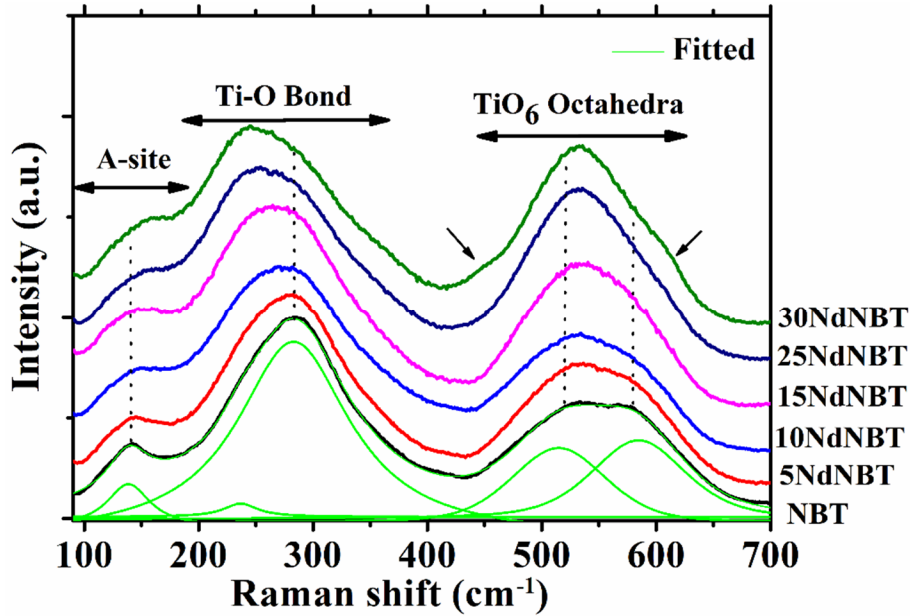


Fig. 4: Room temperature Raman spectra of the x NdNBT ceramics, in addition to the deconvolution of the NBT Raman spectrum.

Fig. 4 shows room temperature Raman spectra recorded from 90 to 700 cm^{-1} for all x NdNBT compositions to probe the structural changes. Remind that the pure compound crystallizes in the rhombohedral ($R3c$) structure. The deconvolution of the Raman modes of the NBT system presents four major Raman peaks situated at 139, 283, 514, and 583 cm^{-1} , in good agreement with other published reports [53–58]. The first vibrational mode ($\nu_1 = 139\text{ cm}^{-1}$) of the A-site of the ABO_3 perovskite, becomes broader with the introduction of Nd^{3+} , due to the increase of the disorder in the A-site. The vibrational mode attributed to the Ti-O vibrations ($\nu_2 = 283\text{ cm}^{-1}$) is also seen to broaden in addition to a clear downshift while increasing neodymium introduction. The higher frequency modes ($\nu_3 = 514\text{ cm}^{-1}$, and $\nu_4 = 583\text{ cm}^{-1}$) are attributed to the TiO_6 octahedral vibrations [59]. The former Raman modes are, in our case, indicative of the structural change. As first observed, two Raman peaks of equal magnitude can be seen in the pure NBT system. With neodymium doping (5%), the ratio (ν_3 / ν_4) is observed to increase slowly. However, further neodymium introduction (10%, 15%) resulted in a drastic decrease of the ν_4 mode with a predominance of ν_3 . At 25% Nd^{3+} , we can observe a merging of the high-frequency Raman modes, which confirms the structural change, with an evolution from a

low to a higher symmetry. Concerning the highest Nd^{3+} composition ($> 25\%$), it is seen from the spectra that additional shoulder modes appear around 445 cm^{-1} , and 608 cm^{-1} , which might be attributed to the low-intensity secondary phases observed previously by the X-ray diffraction technique.

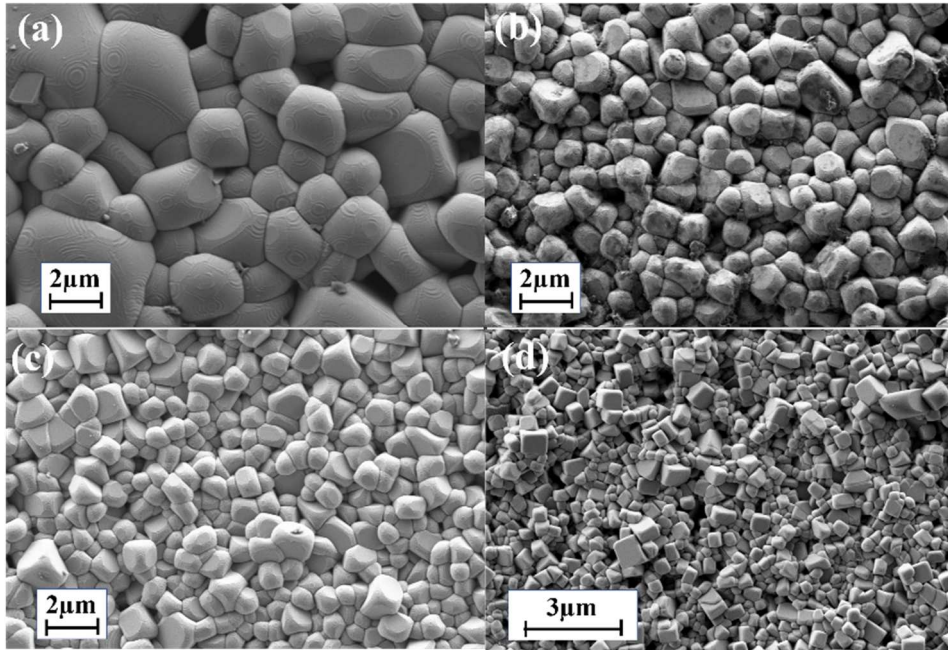


Fig. 5: SEM images of $x\text{NdNBT}$ ceramics with (a) $x = 0$, (b) $x = 5\%$, (c) $x = 10\%$, (d) $x = 30\%$.

Fig. 5(a–d) present the SEM micrographs of $x\text{NdNBT}$ ceramics ($x = 0, 5, 10, 30\%$) in order to illustrate the compositions in different phases ($R3c$, $R3c+Pnma$, and $P4/mmm$). The morphologies of all studied ceramics showed a homogeneous and dense grain microstructure. Interestingly, the pure NBT, 5%, and 10% doping concentrations exhibited spherical-like grain distribution while for high concentrations, $x \geq 25\%$, a morphological change to cubic-like grains is observed, which confirms the symmetry change observed in the XRD investigation. As observed, neodymium introduction impacts drastically the grain size of the studied compounds. NBT system is observed to have grain sizes ranging from 3 to 4 μm . However, with increasing Nd^{3+} concentration, the grain size was reduced to 1–2 μm for the compositions with $x = 5$ and 10%. With further doping ($x = 30\%$), the grain size decreased even more to reach values of 0.5 – 1 μm . The high density and low grain size in ceramics are relevant parameters that can result in an enhanced breakdown strength in the samples.

3.2. Dielectric properties

Fig. 6(a–e) present the temperature dependence of the dielectric permittivity of $x\text{NdNBT}$ ceramics ($x = 0 - 30\%$) measured at different frequencies. From high to low temperatures, the parent NBT system is observed to undergo three dielectric anomalies, namely, $T_m \sim 345^\circ\text{C}$, $T_1 \sim 315^\circ\text{C}$, and $T_d \sim 250^\circ\text{C}$. The first diffuse phase transition at T_m is related to the tetragonal ($P4bm$) to orthorhombic ($Pnma$) transition. Here, T_m represents the temperature of the maximum dielectric permittivity. The NBT system transforms from a rhombohedral to a modulated phase ($R3c + Pnma$) near the depolarization temperature T_d ($\sim 200^\circ\text{C} - 280^\circ\text{C}$).

Therefore, the dielectric anomaly at T_1 is assigned to the transition from the modulated phase to the complete structural change to the orthorhombic ($Pnma$) structure [60,61]. The depolarization temperature where the modulated structure takes place is interesting from a nanoscale point of view. Several NBT-based systems reported on a significant frequency dispersion around T_d which is usually known in relaxor ferroelectric materials and brings to light the dynamic of the polar nanoregions in the system [62–64]. A first observation on the effect of neodymium introduction is the overall decrease of the maximum dielectric permittivity, from 2700 (NBT) to 550 (30NdNBT). Interestingly, the introduction of Nd^{3+} into the NBT matrix up to 10%, increases the room temperature dielectric permittivity from 500 to about 800. By further increasing the doping level, the room temperature dielectric permittivity of 30NdNBT decreases to about 525 but remains higher than the pure NBT.

Neodymium introduction is observed to affect all three dielectric anomalies. Regarding the composition with 5% neodymium doping (Fig. 6(b)), the maximum temperature anomaly is observed to shift to higher temperatures ($T_m \sim 420^\circ\text{C}$) and became further diffuse. In contrast, the T_1 anomaly shifted to lower temperatures ($T_1 \sim 310^\circ\text{C}$) and became more prominent than that of the pure compound. The most interesting effect of neodymium introduction is observed on the depolarization temperature. A broad T_d anomaly covering a large temperature range from room temperature up to 250°C is observed for the 5NdNBT composition. We believe that neodymium introduction increased considerably the relaxor properties of NBT system and thereby increased the PNRs in the structure on a large temperature range. Thence, the substitution of Bi^{3+} with Nd^{3+} resulted in a perturbation of the ferroelectric order and led to the formation of a short-range ergodic relaxor phase. Similar behavior was found by Zhou *et al.* in their recent work, where they reported that the increase of $(Li_{0.5}Nd_{0.5})^{2+}$ concentration in the $(Na_{0.5}Bi_{0.5})^{2+}$ A-site of NBT-12BT system, lead to the prevention of the long-range ferroelectric order and instead promotes the formation of PNRs within the system [65].

Regarding the 10NdNBT composition, a broad plateau-like is observed over a broad range of about 300°C , which is mainly due to the enhanced relaxor character and to the largely diffuse T_m anomaly. The T_1 anomaly of this last composition was observed to downshift to $T_1 \sim 190^\circ\text{C}$. We surmise that the coexistence of $R3c$ and $Pnma$ phases can be found for temperatures below the T_1 anomaly. The former assertion is in good agreement with the Rietveld refinement results. Concerning the composition with 15% of doping, the T_m anomaly is observed to decrease considerably in intensity compared to the diffuse anomaly at 150°C .

Finally, for the highest neodymium concentration, the dielectric anomalies at T_m and T_1 seem to disappear, and only one broad dielectric anomaly is observed at room temperature presenting a strong frequency dispersion. The diffuse character of the dielectric anomaly can be related to the increase of the structural disorder caused by the substitution of Bi^{3+} by Nd^{3+} . Besides, considerably lower dielectric losses were observed for the NdNBT system compared to NBT, particularly at high temperatures (Fig. 6(f)). The very low dielectric losses at high temperatures (ex: 0.044 at 200°C for 5%Nd) combined with high-temperature dielectric stability are significant for high-temperature applications [66].

In recent years, there has been an increasing demand for reliable high-temperature electronics (HTPE) that can operate in a harsh environment, be adapted to space constraints, have high-temperature stability and reliability, and finally can be produced at acceptable costs [67,68]. The former electronics are highly needed in diverse applications, such as in power factor,

microwave communications, hybrid electric vehicles, pulsed power applications, deep-well oil and gas exploration, and also in aerospace systems and NASA space applications [68].

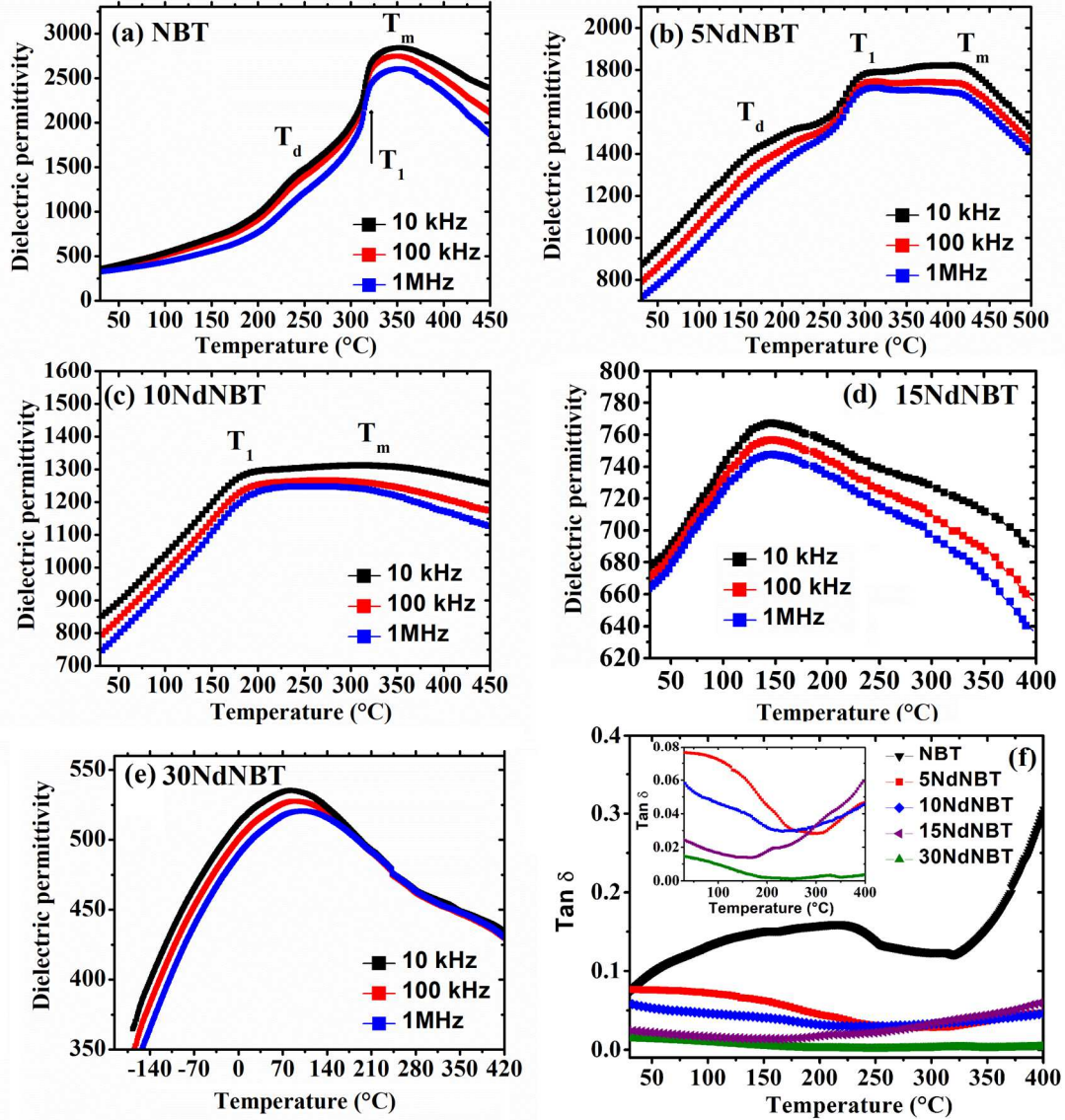


Fig. 6: Dielectric permittivity at 10kHz, 100kHz, and 1MHz of xNdNBT ceramics, with (a) $x = 0$, (b) $x = 5\%$, (c) $x = 10\%$, and (d) $x = 30\%$. (e) Dielectric losses at 100kHz of the compositions with $x = 0 - 30\%$.

Thenceforth, to consider the temperature dielectric stability performances of the xNdNBT system and evaluate the effect of doping on the stability, we introduced a parameter defined as the temperature coefficient of capacitance (TCC), given by the following equation:

$$TCC = \frac{\Delta C}{C_{\text{Base Temp}}} = \frac{\Delta \epsilon_r}{\epsilon_{\text{Base Temp}}} = \frac{\epsilon_T - \epsilon_{\text{Base Temp}}}{\epsilon_{\text{Base Temp}}} \quad (1)$$

The base temperature was taken at 150°C, to cover the majority of high-temperature applications. Fig. 7 shows the temperature change of the capacitance of xNdNBT ceramics as a function of temperature.

Regarding the ceramic with low neodymium doping (5NdNBT), a dielectric temperature stability of $\pm 15\%$ is observed in a small range of temperatures between 100°C and 220°C. However, by increasing the Nd^{3+} concentration, high dielectric temperature stability is

observed over an extensive temperature range. The 10NdNBT composition exhibited a TCC of $\pm 11\%$ from 110°C up to 505°C. In contrast, the 15NdNBT composition presents a TCC of $\pm 15\%$ from room temperature to 400°C. Regarding the 30NdNBT sample, a TCC of $\pm 15\%$ in the range from -90°C to 405°C was found, in addition to a very small TCC of about $< \pm 5\%$ in the temperature range from -30°C to 230°C. Such characteristics are promising for dielectric capacitor applications working around RT and at relatively high temperatures ($< 200^\circ\text{C}$).

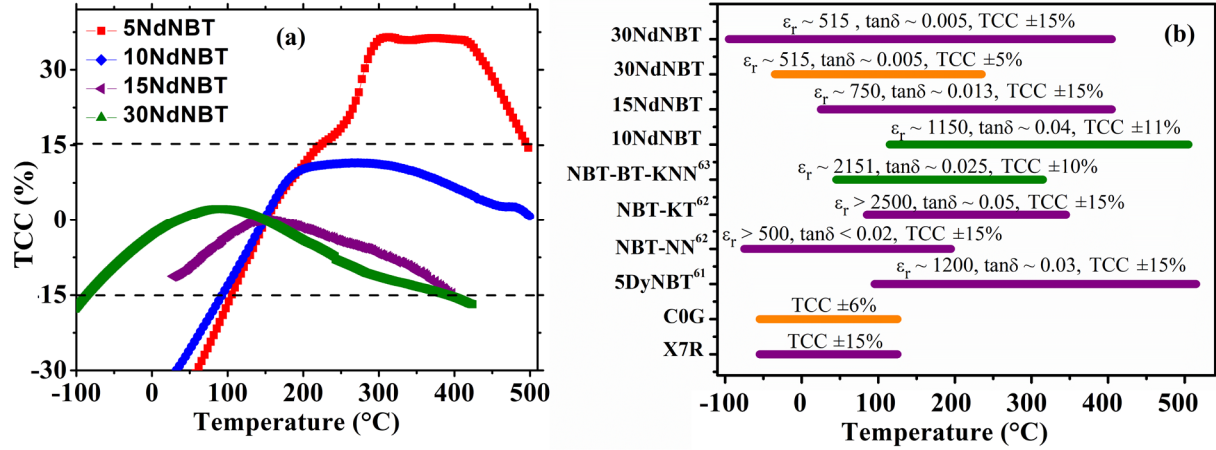


Fig. 7: (a) Temperature change of the capacitance for xNdNBT ceramics at 100kHz with $x = 5, 10, 15$ and 30% . (b) Temperature range stability of the dielectric permittivity of xNdNBT ceramics along with reported data [69–71].

Fig. 7(b) gathers the TCC parameters obtained in this work compared with the standard capacitors and some other NBT-based materials. Conventional power capacitors are generally designed to withstand a maximum temperature of 125°C . The former temperature limit constitutes a hindrance to the long-term reliability of power electronics and also doesn't cover many application sectors, such as deep-well oil and gas exploration ($>200^\circ\text{C}$), combustion sensing ($200 - 300^\circ\text{C}$), and exhaust sensing ($>500^\circ\text{C}$) [72]. In the present work, we succeeded in achieving a much higher maximum temperature stability, superior to 200°C in the studied xNdNBT ceramics, reaching 505°C for 10NdNBT.

3.3. Ferroelectric and energy storage properties

Fig. 8(a-d) presents the room temperature hysteresis loops of the different xNdNBT compositions, in addition to their respective $I(E)$ curves measured under an electric field of 95 kV/cm . Interestingly, while increasing neodymium doping, different relaxor ferroelectric states could be stabilized. The NBT system presents a typical ferroelectric response to the applied electric field, with a square hysteresis loop and two typical current peaks $\pm I_1$, assigned to the electric field induced long-range ferroelectric domain switching. The permanently induced long-range order in non-ergodic relaxor ferroelectric ceramics was reported by several research groups in NBT-based systems. A similar response was found on NBT-KN and NBT-NN systems at specific amounts of substitution [62,73]. Interestingly, the 5NdNBT composition, present four current peaks $\pm I_1$, and $\pm I_2$ at the electric fields of $\pm E_1$ and $\pm E_2$, respectively. The appearance of four peaks in the $I(E)$ curves of 5NdNBT ceramic is a signature of the coexistence of both long-range FE order and PNRs in the system. For such systems, the initially disordered PNRs will align with the applied electric field inducing the

growth of long-range ferroelectric domains, giving rise to a domain switching current ($+I_1$). Once a backward electric field is applied, the induced FE domains from the initial ER phases will first decompose back to PNRs ($-I_2$). Thence at a higher inverse applied electric field, the PNRs will transform again to FE domains ($-I_1$).

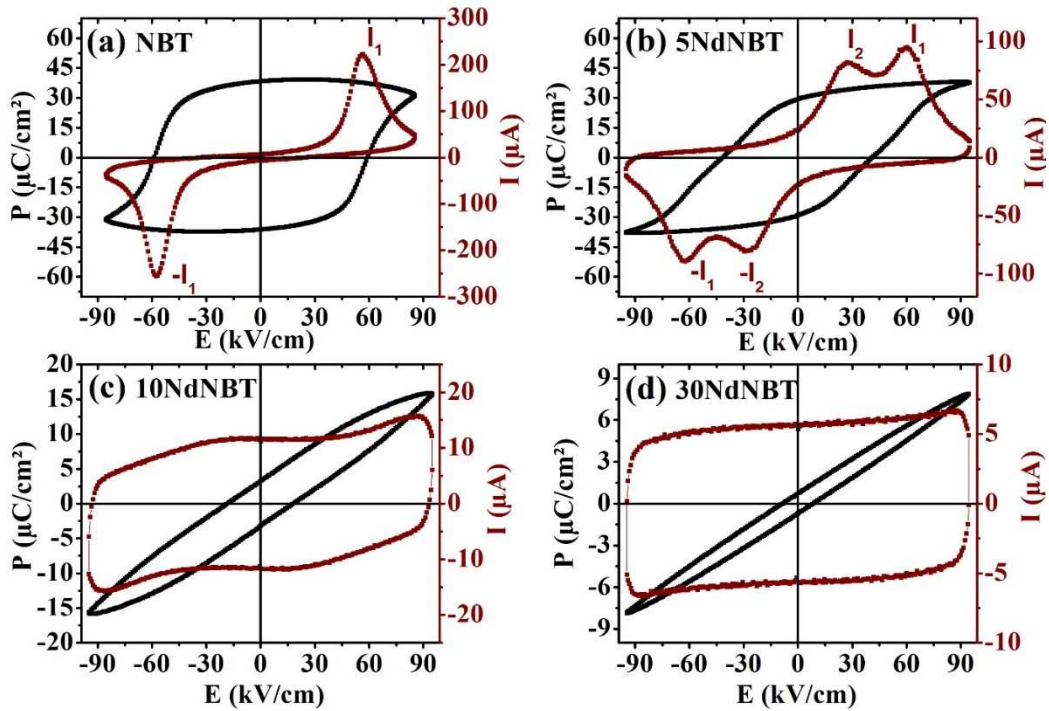


Fig. 8: Room temperature hysteresis loops, in addition to the current versus electric field curves for x NdNBT ceramics, with (a) $x = 0$, (b) $x = 5\%$, (c) $x = 10\%$, (d) $x = 30\%$.

A recent in-situ TEM investigation demonstrated that the I_1 peak in the $I(E)$ curves corresponds to the relaxor-ferroelectric transition with the growth of the PNRs into large FE domains. Furthermore, they reported that the I_2 peak is a signature of the ferroelectric-relaxor transition with the decomposition of the ferroelectric domains into nanodomains [74].

Regarding the composition with 10% Nd^{3+} doping, a slim hysteresis loop is observed with a low remanent polarization and coercive field, and a relatively high maximum polarization. The $I(E)$ curve of such composition makes us believe that the system is in a dominant ergodic phase, with the appearance of only two broad switching current peaks (Fig. 8(c)).

The introduction of a higher doping concentration ($x = 30\%$), results in an increased disorder in the structure, and consequently, the relaxor behavior is amplified and the ferroelectricity is highly decreased. The square $I(E)$ curve of the former composition is due to the small electric field-induced polarization of the complete ergodic relaxor phase.

These results imply that rare earth doping can be an effective and simple way to tailor the electrical properties of the NBT system. In this study, by using a specific level of Nd doping into the matrix of the initially non-ergodic relaxor NBT, different relaxor ferroelectric states could be stabilized; the coexistence of ER and NER (5NdNBT), ER state in intermediate Nd doping (10NdNBT), and a paraelectric-like state for the higher concentration of Nd (30NdNBT).

The temperature dependence of two compositions was investigated to explore the energy storage performances of x NdNBT ceramics. Fig. 9(a-d) presents the temperature dependence

(25°C – 200°C) of the hysteresis loops and the I(E) curves of the 5NdNBT, and 10NdNBT compositions. The room temperature hysteresis loop of 5NdNBT presents a relatively high remanent polarization (P_r) and coercive field (E_c) with a corresponding maximum polarization (P_m) reaching 38 $\mu\text{C}/\text{cm}^2$. As observed, the P_r and E_c values are decreasing considerably while keeping high P_m values as the temperature increase, resulting in pinched P(E) loops. The pinched hysteresis loops observed at high temperatures are due to the electric field-induced microstructural transformations, where the system returns back to its original ergodic relaxor state during the field unloading [75]. Notice that several researcher groups demonstrated the existence of a ferroelectric-to-relaxor (T_{F-R}) phase transition in NBT-based systems close to T_d [73,76,77]. The latter transition highlights principally the size change of the polar nanodomains, in addition to their increased mobility [78]. In the view to determine the T_{F-R} phase transition of the 5NdNBT compound, the current curves were presented in Fig. 9(b). As observed, four current peaks are seen to evolve as a function of temperature.

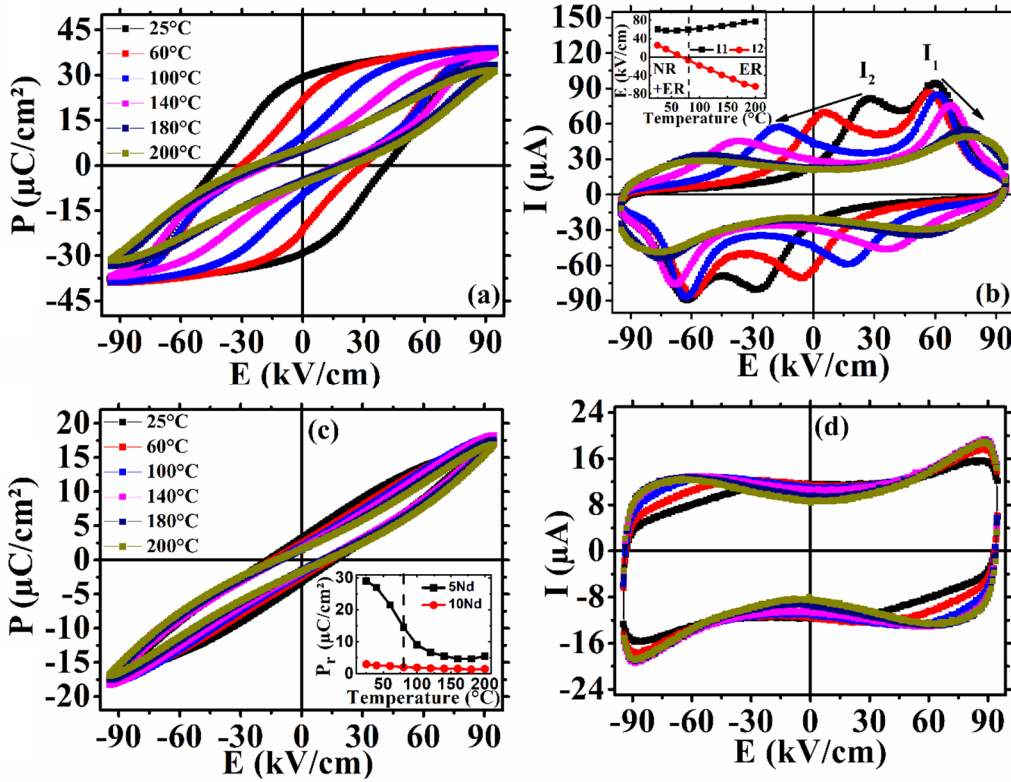


Fig. 9: Temperature-dependent (25 – 200°C) of the hysteresis loops for (a) 5NdNBT, and (c) 10NdNBT ceramics (Inset presents the temperature dependence of P_r for both samples). Temperature-dependent (25 – 200°C) of the I(E) curves for (b) 5NdNBT (Inset shows the temperature evolution of $I_{1,2}$ peaks), and (d) 10NdNBT ceramics.

The temperature evolution of the electric fields E_1 and E_2 corresponding to the current peaks I_1 and I_2 are plotted in the inset of Fig. 9(b). Interestingly, at 80°C, a sign change (from positive to negative) is observed on E_2 suggesting a temperature-induced transition from NER+ER to an ER state. Besides, after a small decrease in I_1 with increasing temperature, it starts to increase back at the critical temperature of 80°C. Therefore, we believe that the T_{F-R} transition in this compound takes place at a temperature of 80°C. Similar behavior was observed by Li *et al.* in NBT-6BT-based ceramics. They reported that the increase of $\text{Sr}_{0.7}\text{Bi}_{0.2}\text{Ti}_{0.1}\text{TiO}_3$ content, makes the I_2 peak emerges in the unloading branch of the J(E)

loops. This feature was reported to be due to the enhanced fraction of ergodic phases in the system and was correlated to the T_{F-R} of the compound [79].

Regarding $x = 10\%$, the temperature dependence of the $P(E)$ loops is captivating, since slim hysteresis loops are obtained with very low E_c and P_r values, in addition to relatively high P_m values. According to these results, we believe that the increase in neodymium doping to $x = 10\%$ resulted in a considerable decrease in the PNRs size (nanometric scale). Similar behavior was observed by Yan *et al.*, in their recent investigation on NBT-BT-based systems [77]. Besides, the increase in temperature resulted in enhanced local random fields and strengthen the ergodic relaxor state in the 10NdNBT ceramic.

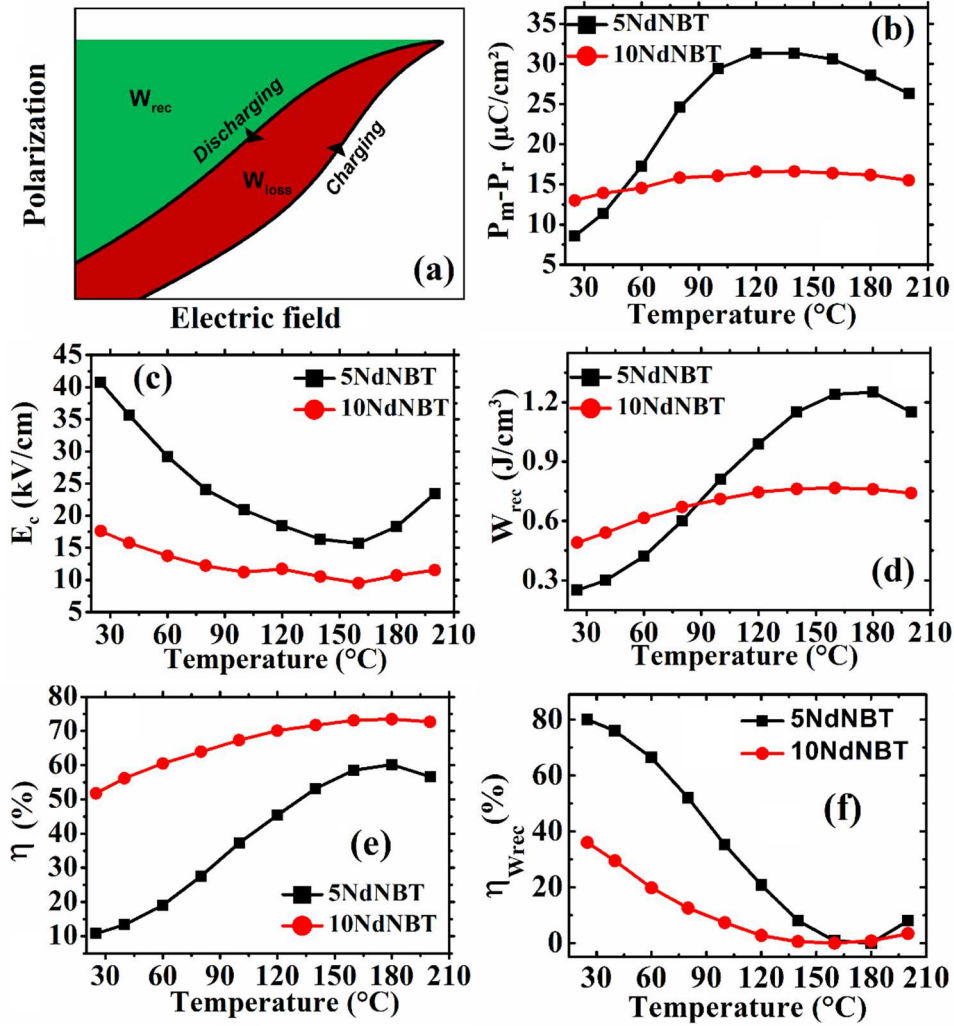


Fig. 10: (a) Definition of the ES parameters. Temperature evolution of (b) $P_m - P_r$, (c) E_c , (d) W_{rec} , (e) η , and (f) W_{rec} instability ($\eta_{W_{rec}}$) of 5NdNBT, and 10NdNBT ceramics.

The remanent polarization of 5NdNBT and 10NdNBT compounds are plotted as a function of temperature in the inset of Fig. 9(c). It can be observed that a much greater P_r value is obtained at room temperature for 5NdNBT compared to the 10NdNBT sample. This feature is demonstrative of the stabilization of the FE order after the removal of the electric field for the 5NdNBT composition. Above 80°C, the P_r value of this last composition illustrates a continuous decrease suggesting that the FE domains could not be further stabilized at high temperatures, and confirms the T_{F-R} temperature for the 5NdNBT system. Besides, the low P_r value of the 10NdNBT sample highlights dominance of the non-stable FE phases after the

removal of the excitation, however a very small portion of stable FE domains still exist in the sample ($P_r \neq 0$) [80].

To assess the ability of our systems to be promoted for energy storage (ES) applications, the temperature dependence of the energy storage density and the energy efficiency were extracted from P-E hysteresis loops of 5NdNBT and 10NdNBT compositions. Remind that the energy storage density (W_{rec}) of a system can be calculated from an integration of the hysteresis loops of the compound (see Fig. 10(a)), and can be written as

$$W_{rec} = \int_{P_r}^{P_m} E dP \quad (2)$$

Accordingly, a high-energy storage density can be obtained for a system presenting a high $\Delta P = P_m - P_r$ value, and having the ability to withstand high applied electric fields. Taking into account the energy dissipated as heat from the system, namely energy losses (W_{loss}), the energy efficiency can be given as follow,

$$\eta = \frac{W_{rec}}{W_{rec} + W_{loss}} \quad (3)$$

To get a clear understanding of the effect of the temperature and doping on the energy storage key parameters, we plotted in Fig. 10(b-e) the temperature evolution of ΔP , E_c , W_{rec} , and η . As we have discussed before, the 5NdNBT ceramic presents a quasi-square ferroelectric hysteresis loop at room temperature, presenting low ΔP , and high E_c values (Fig. 10(b, c)), giving rise to low W_{rec} , and η values (Fig. 10(d, e)). The increase in temperature resulted in an enhancement of the ER phases leading to a considerable rise in the relaxor properties within the system, resulting in a high energy storage density of $W_{rec} = 1.25 \text{ J/cm}^3$ (180°C, and 95 kV/cm), with a corresponding energy efficiency of $\eta = 60\%$.

According to the increased disorder within the 10NdNBT system, prominent relaxor character was noticed from RT to high temperatures. Thenceforth, broad temperature stability was observed over the whole measured temperature range (25°C – 200°C) for the 10NdNBT compound (Fig. 10(b – e)). Consequently, relatively high energy storage density is obtained for the former composition ranging from 0.5 to 0.74 J/cm^3 (25°C - 200°C), with a maximum value of 0.77 J/cm^3 obtained at 160°C. Similarly, the energy storage efficiency also presents high-temperature stability, with a maximum value of $\eta = 73.5\%$ at 180°C.

The temperature stability of the ES performance of a material is essential for practical application. Thus we evaluated the temperature instability of W_{rec} using the following equation [81]:

$$\eta_{W_{rec}} = \frac{W_{recm} - W_{rec}}{W_{recm}} \times 100 \quad (4)$$

Where $\eta_{W_{rec}}$ and W_{recm} present the instability of the energy storage density and the maximum W_{rec} value, respectively. Fig. 10 (f) presents the temperature evolution of $\eta_{W_{rec}}$ for 5NdNBT and 10NdNBT compositions. At low temperatures, the 5NdNBT sample exhibits high $\eta_{W_{rec}}$ values. By increasing the temperature, $\eta_{W_{rec}}$ decreases quasi-linearly before stabilizing at temperatures higher than 120°C. For $T > 100^\circ\text{C}$, $\eta_{W_{rec}}$ is below 20% while a very small instability of $< 8\%$ is reached for $T > 120^\circ\text{C}$. In contrast to the 5NdNBT composition, the 10NdNBT presents low $\eta_{W_{rec}}$ values over the whole studied temperature range, in particular a very small $\eta_{W_{rec}} < 7\%$ between 100 and 200°C is obtained.

Fig. 11 gathers the obtained energy storage densities in the xNdNBT ceramics, along with some reported literature data of NBT-based systems. The obtained results show that rare-earth

doping can be considered as a simple and elegant way to design lead-free relaxor ferroelectric materials with high-energy storage performances operating at high temperatures.

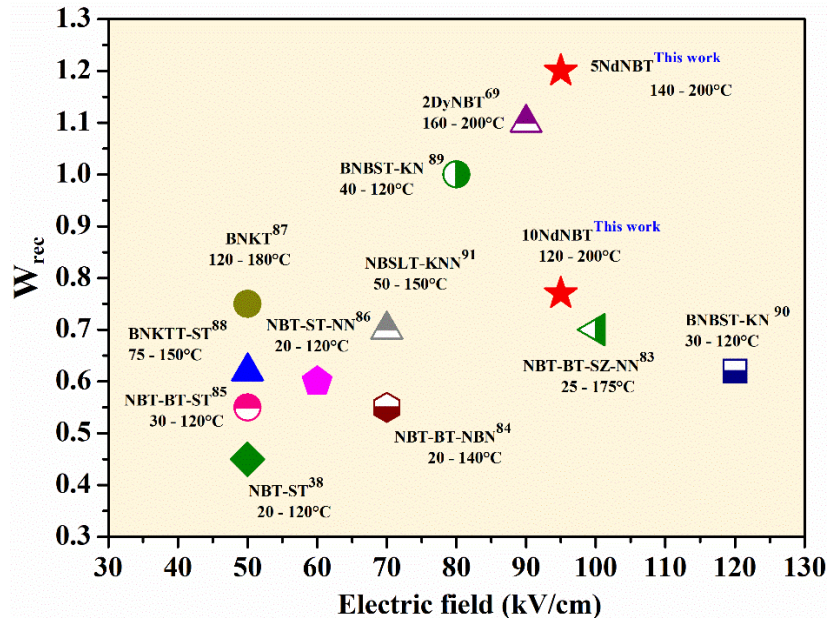


Fig. 11: Energy storage density obtained in this work (represented by stars) in comparison to some literature data of complex NBT-based systems [38,69,83–91].

3.4. Electrocaloric investigations

The electric field applied to a ferroelectric material leads to an increase in the dipolar order and, therefore, to a decrease in entropy. Conversely, removing the electric field allows the material to relax by increasing its entropy. These entropy variations are the origin of a temperature variation called the electrocaloric effect (ECE). In standard ferroelectric material, substantial entropy change could be obtained at the ferroelectric (FE)-paraelectric (PE) phase transition resulting in a narrow ECE peak at the Curie temperature. However, the small temperature stability of ECE in normal ferroelectrics is not suitable for practical applications. In recent years, relaxor ferroelectric materials have attracted considerable interest in cooling technologies owing to their diffuse phase transitions, which are desired for producing high ECE in a broad temperature range [92–94]. For instance, high ECE response in a broad temperature range between T_d and T_m has been reported in the non-ergodic relaxor PZT based system [95].

In the present work, we aim to investigate the ECE response between RT and T_d in the relaxor ferroelectric 5NdNBT ceramic, presenting the coexistence of both NER and ER state at RT. The coexisted phases can result in an enhanced ECE response, which was demonstrated by Li *et al.* in their investigation of the electrocaloric effect in NBT-BT based system [79]. In subsequent work, the authors demonstrated an enhanced ECE in NBT-ST ceramics presenting a freezing temperature near RT [96]. It is believed that the design of lead-free RF materials with different relaxor phases is suitable for high electrocaloric response in a wide temperature range.

The evaluation of the ECE can be obtained through the investigation of the adiabatic temperature change, ΔT , using the indirect method based on the Maxwell equation:

$$\Delta T = -\frac{1}{\rho C_p} \int_{E_i}^{E_f} T \left(\frac{\partial P}{\partial T} \right) dE \quad (5)$$

Where E_i and E_f correspond to the starting and final applied electric fields, $\partial P/\partial T$ represents the pyroelectric coefficient, ρ , and C_p stand for the density (5.97 g/cm^3) and the specific heat capacity (537 J/K Kg) of the 5NdNBT system, respectively.

The temperature evolution of the polarization at different applied electric fields obtained from the upper branch of the P-E hysteresis loops was plotted in Fig. 12(a). For all-electric fields, the polarization exhibits a smooth decrease with the increase in temperature. The former feature highlights the transition from the ferroelectric to the relaxor state and is observed to shift to higher temperatures when the electric field increases. Fig. 12(b) shows the temperature evolution of the ECE of 5NdNBT composition at different applied electric fields (5 – 95 kV/cm). In a ferroelectric compound with a typical FE-PE phase transition, a sharp ΔT peak can be observed near T_c . However, for a relaxor system, the temperature evolution of ΔT depends mainly on the existence of PNRs [97]. A broad ECE response can be obtained for temperatures presenting a significant change in the dynamics of PNRs. For instance, an enhanced EC effect was found in the region of the ferroelectric-to-relaxor phase transition for the NBT-6BT system ($\sim 100^\circ\text{C}$) [76].

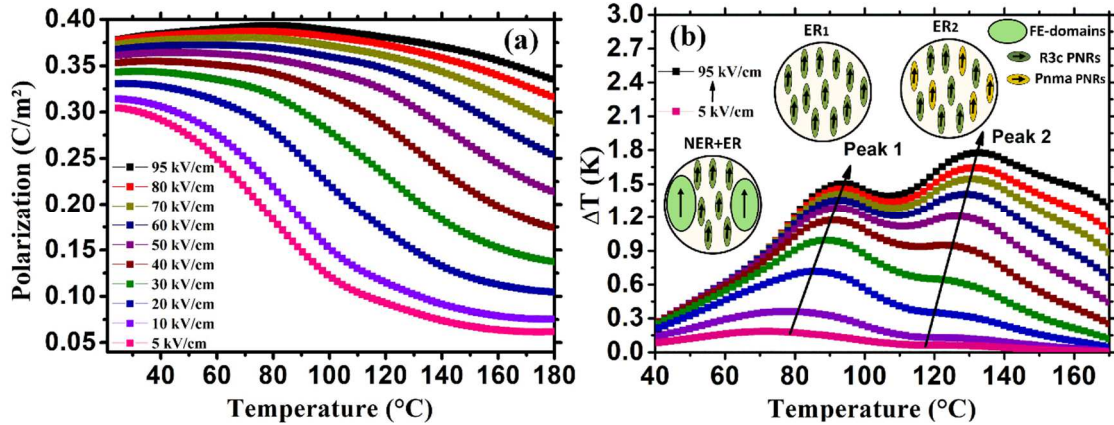


Fig. 12: (a) Temperature dependence of the polarization, (b) electrocaloric temperature change (ΔT) as a function of temperature at different electric fields (inset shows the PNRs behavior as a function of temperature at E_{max}).

At low electric fields below 5 kV/cm, ΔT shows a first broad peak (noted as peak 1) with a maximum $T_{\Delta Tm1}$ around 72°C . By increasing the electric field, the peak 1 becomes less broad and shifts gradually to high temperatures ($T_{\Delta Tm1} = 93^\circ\text{C}$ at 95 kV/cm), while a second peak (noted as peak 2) emerged at 127°C and became perceptible for applied electric fields higher than 10 kV/cm. The intensity of peak 2 increases with the electric field and forms with peak 1 a ‘plateau-like’ ECE for electric fields higher than 40 kV/cm. For $E > 60 \text{ kV/cm}$, the ΔT of peak 2 becomes higher than that of peak 1 and reaches 1.8 K under 95 kV/cm.

For this system, the substitution of Bi^{3+} by a rare earth element (Nd^{3+}) in the ABO_3 perovskite, increases the disorder in the A-site, inducing local random fields which results in the appearance of an ER state at RT that coexist with the initial NER state of the parent NBT system. By increasing the temperature, the local random fields increase within the system with enhanced ergodicity. First, when a small electric field is applied, a weak ECE is obtained corresponding to the polarization reorientation of the PNRs and the transformation of a small

part of PNRs into ferroelectric macrodomains. By applying a sufficient electric field, the relaxor state with short-range-order PNRs transforms into a stable ferroelectric long-range-order. The electric field removal results in a high ECE due to the coexistence of the induced ferroelectric macro-domains and the ER state at $E = 0$.

The first peak obtained around 90°C can be associated with a complete transformation of the ferroelectric NER+ER states to a first relaxor ER state (denoted by ER_1 in Fig. 12(b)). The second ECE peak appearance at about 130°C , could be interpreted by the transformation of the ER_1 to ER_2 with different kinds of PNRs. We believe that while increasing the temperature ($\sim T_d$), $Pnma$ PNRs might manifest in the system along with the $R3c$ PNRs, resulting in a higher entropy variation distinguished by the broad peak 2. For the highest temperatures ($T > 130^\circ\text{C}$), the decrease in the ΔT value is mainly due to the difficulty to reorient the dominant $Pnma$ PNRs in the pure ergodic relaxor state. Relaxor domain states in the electric field as a function of temperature are depicted in the inset of Fig. 13(b).

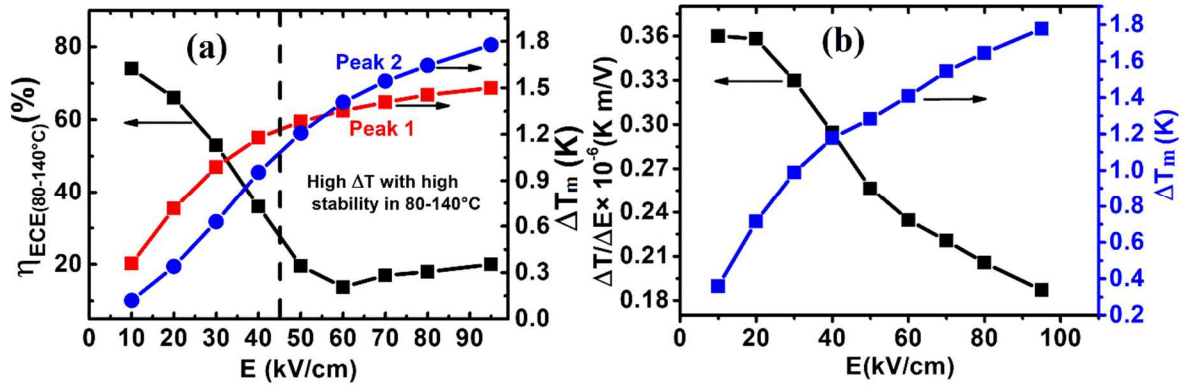


Fig. 13: (a) the ECE instability in the temperature range (80-140°C) and the electric field evolution of ΔT_m for peaks 1 and 2 of 5NdNBT ceramic. (b) The electric field dependence of the ECE responsivity and ΔT_m .

Temperature stability of ECE, a relevant parameter for applications, is given by [81]:

$$\eta_{ECE} = \frac{\Delta T_m - \Delta T}{\Delta T_m} \times 100 \quad (6)$$

Where η_{ECE} presents the electrocaloric instability and ΔT_m stands for the maximum ECE value. Fig. 13(a) shows the electric field evolution of η_{ECE} in the temperature range of 80-140°C, and ΔT_m for peak 1 (ΔT_{m1}) and peak 2 (ΔT_{m2}).

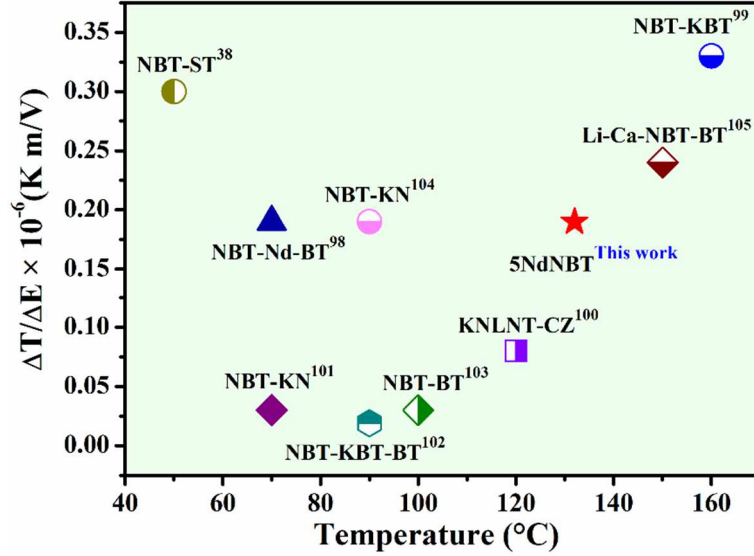


Fig. 14: Comparison of the electrocaloric coefficient obtained in our work with some reported NBT-based systems [38,98–104].

Increasing the electric field from 10 to 95 kV/cm, ΔT_{m1} and ΔT_{m2} increases from 0.36 to 1.5 K and 0.12 to 1.8 K, respectively. At $E = 10$ kV/cm, η_{ECE} is high and exhibits a linear decrease when E increases up to 40 kV/cm before stabilizing at a high electric field. Interestingly, in the electric field range, 40 – 95 kV/cm, the η_{ECE} (80-140°C) shows low instability below 20% accompanied by a higher electrocaloric response ($1.18 \text{ K} \leq \Delta T_m \leq 1.8 \text{ K}$) which is highly desirable for practical applications. To evaluate the performance of the obtained ECE in the studied sample, the responsivity $\Delta T_m/\Delta E$ is plotted in Fig. 13(b) together with ΔT_m as a function of the applied electric field. As we can see from the figure, a high responsivity is obtained of 0.19×10^{-6} when at 95 kV/cm. Figure 14 regroups the obtained EC parameters for 5NdNBT composition and some reported literature data of lead-free NBT-based systems. This work highlights the benefit of inducing NER and ER relaxor states in the NBT system through Nd-doping on the electrocaloric response. We suggest that the increased relaxor state in the 5NdNBT system benefits the electrocaloric response and improves its thermal stability, which is highly needed in cooling technologies.

4. Conclusion

In this work, lead-free relaxor $\text{Na}_{0.5}(\text{Bi}_{1-x}\text{Nd}_x)_{0.5}\text{TiO}_3$ ceramics with different neodymium concentrations ($x = 0, 5\%, 10\%, 15\%, 25\%, 30\%$) were investigated. XRD and SEM investigations revealed a pure perovskite phase and dense microstructure for the studied compounds. Structural transformations were noticed as a function of Nd^{3+} doping. By increasing neodymium content, the structure changes from a rhombohedral $R3c$, rhombohedral $R3c$ + orthorhombic $Pnma$, and finally to a tetragonal $P4/mmm$ structure. Dielectric investigations revealed very low dielectric losses in the doped compounds. Besides, the introduction of the Nd^{3+} element was seen to induce a strong frequency dispersion in the $\epsilon_r(T)$ curve, highlighting the presence of PNRs within the doped compositions. A stable TCC ($\leq \pm 15\%$) over a wide temperature range with a maximum working temperature exceeding 200°C was observed for all doped compositions, which makes the $x\text{NdNBT}$ ceramics potential candidates for reliable high-temperature electronics. Besides, considerable energy

storage properties were obtained for xNdNBT ceramics, with $W_{\text{rec}} > 1.14 \mu\text{C}/\text{cm}^2$ ($140^\circ\text{C} - 200^\circ\text{C}$) for 5NdNBT ceramic, and $W_{\text{rec}} > 0.75 \mu\text{C}/\text{cm}^2$ ($120^\circ\text{C} - 200^\circ\text{C}$) at 95 kV/cm for 10NdNBT ceramic. In addition, an enhanced ECE was obtained for the 5%Nd composition, with $\Delta T = 1.8 \text{ K}$ at 95 kV/cm and a corresponding low ΔT instability below 20% over a broad temperature range ($80 - 140^\circ\text{C}$). Through the investigation of the $\Delta T(T)$ curve, we proposed a schematic representation of the temperature effect on the PNRs (5NdNBT system). We believe that Nd^{3+} doping can be a powerful tool to tailor the local nanostructure of the NBT system and its dielectric, ferroelectric, energy storage and electrocaloric properties.

Acknowledgments

Financial support by the Haute France Region/FEDER (project MASENE), Slovenian Research Agency (programs P1-0125 and P2-0091) and H2020-RISE-ENGIMA (No. 778072) project are gratefully acknowledged.

References

- [1] G. Smolensky, Ferroelectrics with diffuse phase transition, *Ferroelectrics*. 53 (1984) 129–135. <https://doi.org/10.1080/00150198408245041>.
- [2] A. Safari, E.K. Akdogan, eds., *Piezoelectric and acoustic materials for transducer applications*, Springer, New York, 2008.
- [3] S.-E. Park, T.R. Shrout, Ultrahigh strain and piezoelectric behavior in relaxor based ferroelectric single crystals, *Journal of Applied Physics*. 82 (1997) 1804–1811. <https://doi.org/10.1063/1.365983>.
- [4] T. Badapanda, S.K. Rout, L.S. Cavalcante, J.C. Sczancoski, S. Panigrahi, E. Longo, M.S. Li, Optical and dielectric relaxor behaviour of $\text{Ba}(\text{Zr}_{0.25}\text{Ti}_{0.75})\text{O}_3$ ceramic explained by means of distorted clusters, *J. Phys. D: Appl. Phys.* 42 (2009) 175414. <https://doi.org/10.1088/0022-3727/42/17/175414>.
- [5] A.A. Bokov, Z.-G. Ye, Phenomenological description of dielectric permittivity peak in relaxor ferroelectrics, *Solid State Communications*. 116 (2000) 105–108. [https://doi.org/10.1016/S0038-1098\(00\)00295-7](https://doi.org/10.1016/S0038-1098(00)00295-7).
- [6] N. Setter, L.E. Cross, The role of B-site cation disorder in diffuse phase transition behavior of perovskite ferroelectrics, *Journal of Applied Physics*. 51 (1980) 4356–4360. <https://doi.org/10.1063/1.328296>.
- [7] W. Jo, T. Granzow, E. Aulbach, J. Rödel, D. Damjanovic, Origin of the large strain response in $(\text{K}_{0.5}\text{Na}_{0.5})\text{NbO}_3$ -modified $(\text{Bi}_{0.5}\text{Na}_{0.5})\text{TiO}_3$ - BaTiO_3 lead-free piezoceramics, *Journal of Applied Physics*. 105 (2009) 094102. <https://doi.org/10.1063/1.3121203>.
- [8] S.-T. Zhang, A.B. Kounga, E. Aulbach, T. Granzow, W. Jo, H.-J. Kleebe, J. Rödel, Lead-free piezoceramics with giant strain in the system $\text{Bi}_{0.5}\text{Na}_{0.5}\text{TiO}_3$ - BaTiO_3 - $\text{K}_{0.5}\text{Na}_{0.5}\text{NbO}_3$. I. Structure and room temperature properties, *Journal of Applied Physics*. 103 (2008) 034107. <https://doi.org/10.1063/1.2838472>.
- [9] W. Jo, R. Dittmer, M. Acosta, J. Zang, C. Groh, E. Sapper, K. Wang, J. Rödel, Giant electric-field-induced strains in lead-free ceramics for actuator applications – status and perspective, *J Electroceram.* 29 (2012) 71–93. <https://doi.org/10.1007/s10832-012-9742-3>.
- [10] J. Li, R. Yin, X. Su, J. Li, S. Qin, Q. Wei, M. Zhu, D. Guo, L. Qiao, Y. Bai, Composition-induced non-ergodic–ergodic transition and electrocaloric evolution in $\text{Pb}_{1-1.5x}\text{LaxZr}_{0.8}\text{Ti}_{0.2}\text{O}_3$ relaxor ferroelectric ceramics, *IET Nanodielectrics*. 2 (2019) 123–128. <https://doi.org/10.1049/iet-nde.2019.0001>.

- [11] G. Burns, F.H. Dacol, Glassy polarization behavior in ferroelectric compounds $\text{Pb}(\text{Mg}_{13}\text{Nb}_{23})\text{O}_3$ and $\text{Pb}(\text{Zn}_{13}\text{Nb}_{23})\text{O}_3$, *Solid State Communications*. 48 (1983) 853–856. [https://doi.org/10.1016/0038-1098\(83\)90132-1](https://doi.org/10.1016/0038-1098(83)90132-1).
- [12] J. Macutkevic, S. Kamba, K. Glemza, J. Banys, K. Bormanis, A. Sternberg, High Temperature Dielectric Properties of PMN-PSN-PZN Relaxors, *Physica Status Solidi (b)*. 256 (2019) 1900050. <https://doi.org/10.1002/pssb.201900050>.
- [13] C. Li, B. Xu, D. Lin, S. Zhang, L. Bellaiche, T.R. Shrout, F. Li, Atomic-scale origin of ultrahigh piezoelectricity in samarium-doped PMN-PT ceramics, *Phys. Rev. B*. 101 (2020) 140102. <https://doi.org/10.1103/PhysRevB.101.140102>.
- [14] X. Wang, L. Zhang, X. Hao, S. An, High energy-storage performance of $0.9\text{Pb}(\text{Mg}_{1/3}\text{Nb}_{2/3})\text{O}_3$ - 0.1PbTiO_3 relaxor ferroelectric thin films prepared by RF magnetron sputtering, *Materials Research Bulletin*. 65 (2015) 73–79. <https://doi.org/10.1016/j.materresbull.2015.01.038>.
- [15] K. Yao, S. Chen, M. Rahimabady, M.S. Mirshekarloo, S. Yu, F.E.H. Tay, T. Sritharan, L. Lu, Nonlinear dielectric thin films for high-power electric storage with energy density comparable with electrochemical supercapacitors, *IEEE Transactions on Ultrasonics, Ferroelectrics, and Frequency Control*. 58 (2011) 1968–1974. <https://doi.org/10.1109/TUFFC.2011.2039>.
- [16] Directive 2011/65/EU of the European Parliament and of the Council of 8 June 2011 on the restriction of the use of certain hazardous substances in electrical and electronic equipment Text with EEA relevance, 2011. <http://data.europa.eu/eli/dir/2011/65/oj/eng> (accessed February 13, 2020).
- [17] Z. Pan, D. Hu, Y. Zhang, J. Liu, B. Shen, J. Zhai, Achieving high discharge energy density and efficiency with NBT-based ceramics for application in capacitors, *J. Mater. Chem. C*. 7 (2019) 4072–4078. <https://doi.org/10.1039/C9TC00087A>.
- [18] A.P. Sharma, D.K. Pradhan, S.K. Pradhan, M. Bahoura, Large energy storage density performance of epitaxial BCT/BZT heterostructures via interface engineering, *Scientific Reports*. 9 (2019) 1–8. <https://doi.org/10.1038/s41598-019-53358-0>.
- [19] D. Wang, Z. Fan, D. Zhou, A. Khesro, S. Murakami, A. Feteira, Q. Zhao, X. Tan, I. M. Reaney, Bismuth ferrite-based lead-free ceramics and multilayers with high recoverable energy density, *Journal of Materials Chemistry A*. 6 (2018) 4133–4144. <https://doi.org/10.1039/C7TA09857J>.
- [20] G. Wang, J. Li, X. Zhang, Z. Fan, F. Yang, A. Feteira, D. Zhou, D.C. Sinclair, T. Ma, X. Tan, D. Wang, I.M. Reaney, Ultrahigh energy storage density lead-free multilayers by controlled electrical homogeneity, *Energy Environ. Sci*. 12 (2019) 582–588. <https://doi.org/10.1039/C8EE03287D>.
- [21] G. Wang, Z. Lu, H. Yang, H. Ji, A. Mostaed, L. Li, Y. Wei, A. Feteira, S. Sun, D. C. Sinclair, D. Wang, I. M. Reaney, Fatigue resistant lead-free multilayer ceramic capacitors with ultrahigh energy density, *Journal of Materials Chemistry A*. 8 (2020) 11414–11423. <https://doi.org/10.1039/D0TA00216J>.
- [22] Z. Lu, G. Wang, W. Bao, J. Li, L. Li, A. Mostaed, H. Yang, H. Ji, D. Li, A. Feteira, F. Xu, D. C. Sinclair, D. Wang, S.-Y. Liu, I. M. Reaney, Superior energy density through tailored dopant strategies in multilayer ceramic capacitors, *Energy & Environmental Science*. 13 (2020) 2938–2948. <https://doi.org/10.1039/D0EE02104K>.
- [23] G. Liu, Y. Li, M. Shi, L. Yu, P. Chen, K. Yu, Y. Yan, L. Jin, D. Wang, J. Gao, An investigation of the dielectric energy storage performance of $\text{Bi}(\text{Mg}_{2/3}\text{Nb}_{1/3})\text{O}_3$ -modified BaTiO_3 Pb-free bulk ceramics with improved temperature/frequency stability, *Ceramics International*. 45 (2019) 19189–19196. <https://doi.org/10.1016/j.ceramint.2019.06.166>.
- [24] G. Liu, Y. Li, B. Guo, M. Tang, Q. Li, J. Dong, L. Yu, K. Yu, Y. Yan, D. Wang, L. Zhang, H. Zhang, Z. He, L. Jin, Ultrahigh dielectric breakdown strength and excellent energy storage performance in lead-free barium titanate-based relaxor ferroelectric ceramics via a combined strategy of composition modification, viscous polymer processing, and liquid-phase sintering, *Chemical Engineering Journal*. 398 (2020) 125625. <https://doi.org/10.1016/j.cej.2020.125625>.
- [25] H. Yang, Z. Lu, L. Li, W. Bao, H. Ji, J. Li, A. Feteira, F. Xu, Y. Zhang, H. Sun, Z. Huang, W. Lou, K. Song, S. Sun, G. Wang, D. Wang, I.M. Reaney, Novel BaTiO_3 -Based, Ag/Pd-Compatible Lead-

- Free Relaxors with Superior Energy Storage Performance, *ACS Appl. Mater. Interfaces*. 12 (2020) 43942–43949. <https://doi.org/10.1021/acsami.0c13057>.
- [26] W.-B. Li, D. Zhou, W.-F. Liu, J.-Z. Su, F. Hussain, D.-W. Wang, G. Wang, Z.-L. Lu, Q.-P. Wang, High-temperature BaTiO₃-based ternary dielectric multilayers for energy storage applications with high efficiency, *Chemical Engineering Journal*. 414 (2021) 128760. <https://doi.org/10.1016/j.cej.2021.128760>.
- [27] L. Zhang, Z. Wang, Y. Li, P. Chen, J. Cai, Y. Yan, Y. Zhou, D. Wang, G. Liu, Enhanced energy storage performance in Sn doped Sr_{0.6}(Na_{0.5}Bi_{0.5})_{0.4}TiO₃ lead-free relaxor ferroelectric ceramics, *Journal of the European Ceramic Society*. 39 (2019) 3057–3063. <https://doi.org/10.1016/j.jeurceramsoc.2019.02.004>.
- [28] B. Guo, L. Zhang, J. Dong, Y. Li, F. Chen, Q. Ai, Q. Li, Z. He, Y. Yan, D. Wang, Enhanced energy storage properties of ZrO₂-doped (Na_{0.5}Bi_{0.5})_{0.4}Sr_{0.6}TiO₃ Pb-free relaxor ferroelectric ceramics, *Ceramics International*. 47 (2021) 8545–8554. <https://doi.org/10.1016/j.ceramint.2020.11.222>.
- [29] H. Ji, D. Wang, W. Bao, Z. Lu, G. Wang, H. Yang, A. Mostaed, L. Li, A. Feteira, S. Sun, F. Xu, D. Li, C.-J. Ma, S.-Y. Liu, I.M. Reaney, Ultrahigh energy density in short-range tilted NBT-based lead-free multilayer ceramic capacitors by nanodomain percolation, *Energy Storage Materials*. 38 (2021) 113–120. <https://doi.org/10.1016/j.ensm.2021.01.023>.
- [30] V.V. Shvartsman, D.C. Lupascu, Lead-Free Relaxor Ferroelectrics, *Journal of the American Ceramic Society*. 95 (2012) 1–26. <https://doi.org/10.1111/j.1551-2916.2011.04952.x>.
- [31] I.G. Siny, C.-S. Tu, V.H. Schmidt, Critical acoustic behavior of the relaxor ferroelectric $\text{Na}_{1/2}\text{Bi}_{1/2}\text{TiO}_3$ in the intertransition region, *Phys. Rev. B*. 51 (1995) 5659–5665. <https://doi.org/10.1103/PhysRevB.51.5659>.
- [32] P.K. Davies, H. Wu, A.Y. Borisevich, I.E. Molodetsky, L. Farber, Crystal Chemistry of Complex Perovskites: New Cation-Ordered Dielectric Oxides, *Annual Review of Materials Research*. 38 (2008) 369–401. <https://doi.org/10.1146/annurev.matsci.37.052506.084356>.
- [33] M. Gröting, S. Hayn, K. Albe, Chemical order and local structure of the lead-free relaxor ferroelectric Na_{1/2}Bi_{1/2}TiO₃, *Journal of Solid State Chemistry*. 8 (2011) 2041–2046. <https://doi.org/10.1016/j.jssc.2011.05.044>.
- [34] Z. Chen, J. Hu, Piezoelectric and dielectric properties of (Bi_{0.5}Na_{0.5})_{0.94}Ba_{0.06}TiO₃–Ba(Zr_{0.04}Ti_{0.96})O₃ lead-free piezoelectric ceramics, *Ceramics International*. 35 (2009) 111–115. <https://doi.org/10.1016/j.ceramint.2007.09.110>.
- [35] C. Peng, J.-F. Li, W. Gong, Preparation and properties of (Bi_{1/2}Na_{1/2})TiO₃–Ba(Ti,Zr)O₃ lead-free piezoelectric ceramics, *Materials Letters*. 59 (2005) 1576–1580. <https://doi.org/10.1016/j.matlet.2005.01.026>.
- [36] Y. Li, W. Chen, Q. Xu, J. Zhou, X. Gu, Piezoelectric and ferroelectric properties of Na_{0.5}Bi_{0.5}TiO₃–K_{0.5}Bi_{0.5}TiO₃–BaTiO₃ piezoelectric ceramics, *Materials Letters*. 59 (2005) 1361–1364. <https://doi.org/10.1016/j.matlet.2004.12.041>.
- [37] D. Lin, K.W. Kwok, Dielectric and piezoelectric properties of (Bi_{1-x-y}Nd_xNa_{1-y})_{0.5}BayTiO₃ lead-free ceramics, *Current Applied Physics*. 10 (2010) 422–427. <https://doi.org/10.1016/j.cap.2009.06.044>.
- [38] W.P. Cao, W.L. Li, X.F. Dai, T.D. Zhang, J. Sheng, Y.F. Hou, W.D. Fei, Large electrocaloric response and high energy-storage properties over a broad temperature range in lead-free NBT-ST ceramics, *Journal of the European Ceramic Society*. 36 (2016) 593–600. <https://doi.org/10.1016/j.jeurceramsoc.2015.10.019>.
- [39] H. Guo, Y. Li, Y. Zhang, H. Sun, X. Liu, Improved electrical properties of Co-doped 0.92NBT–0.04KBT–0.04BT lead-free ceramics, *J Mater Sci: Mater Electron*. 29 (2018) 19063–19069. <https://doi.org/10.1007/s10854-018-0032-y>.
- [40] G. Wang, Z. Lu, Z. Zhang, A. Feteira, C.C. Tang, D.A. Hall, Electric field-induced irreversible relaxor to ferroelectric phase transformations in Na_{0.5}Bi_{0.5}TiO₃–NaNbO₃ ceramics, *Journal of the American Ceramic Society*. 102 (2019) 7746–7754. <https://doi.org/10.1111/jace.16676>.

- [41] M. Otonicar, J. Park, M. Logar, G. Esteves, J.L. Jones, B. Jancar, External-field-induced crystal structure and domain texture in $(1-x)\text{Na}_0.5\text{Bi}_0.5\text{TiO}_3-x\text{K}_0.5\text{Bi}_0.5\text{TiO}_3$ piezoceramics, *Acta Materialia*. 127 (2017) 319–331. <https://doi.org/10.1016/j.actamat.2017.01.052>.
- [42] S.R. Kanuru, K. Baskar, R. Dhanasekaran, Synthesis, structural, morphological and electrical properties of NBT–BT ceramics for piezoelectric applications, *Ceramics International*. 42 (2016) 6054–6064. <https://doi.org/10.1016/j.ceramint.2015.12.162>.
- [43] M. Zannen, A. Lahmar, B. Asbani, H. Khemakhem, M. El Marssi, Z. Kutnjak, M. Es Souni, Electrocaloric effect and luminescence properties of lanthanide doped $(\text{Na}_{1/2}\text{Bi}_{1/2})\text{TiO}_3$ lead free materials, *Appl. Phys. Lett.* 107 (2015) 032905. <https://doi.org/10.1063/1.4927280>.
- [44] M. Zannen, A. Lahmar, M. Dietze, H. Khemakhem, A. Kabadou, M. Es-Souni, Structural, optical, and electrical properties of Nd-doped $\text{Na}_0.5\text{Bi}_0.5\text{TiO}_3$, *Materials Chemistry and Physics*. 134 (2012) 829–833. <https://doi.org/10.1016/j.matchemphys.2012.03.076>.
- [45] M. Benyoussef, M. Zannen, J. Belhadi, B. Manoun, J.-L. Dellis, A. Lahmar, M. El Marssi, Complex impedance and Raman spectroscopy of $\text{Na}_0.5(\text{Bi}_{1-x}\text{Dy}_x)_0.5\text{TiO}_3$ ceramics, *Ceramics International*. 46 (2020) 10979–10991. <https://doi.org/10.1016/j.ceramint.2020.01.114>.
- [46] M. Zannen, A. Lahmar, Z. Kutnjak, J. Belhadi, H. Khemakhem, M. El Marssi, Electrocaloric effect and energy storage in lead free $\text{Gd}_0.02\text{Na}_0.5\text{Bi}_0.48\text{TiO}_3$ ceramic, *Solid State Sciences*. 66 (2017) 31–37. <https://doi.org/10.1016/j.solidstatesciences.2017.02.007>.
- [47] J. Chen, H.M. Chan, M.P. Harmer, Ordering Structure and Dielectric Properties of Undoped and La/Na-Doped $\text{Pb}(\text{Mg}_{1/3}\text{Nb}_{2/3})\text{O}_3$, *Journal of the American Ceramic Society*. 72 (1989) 593–598. <https://doi.org/10.1111/j.1151-2916.1989.tb06180.x>.
- [48] G.A. Samara, The relaxational properties of compositionally disordered ABO_3 perovskites, *J. Phys.: Condens. Matter*. 15 (2003) R367–R411. <https://doi.org/10.1088/0953-8984/15/9/202>.
- [49] W. Kleemann, Relaxor ferroelectrics: Cluster glass ground state via random fields and random bonds, *Physica Status Solidi B Basic Research*. 251 (2014) 1993–2002. <https://doi.org/10.1002/pssb.201350310>.
- [50] A. Deng, J. Wu, Effects of rare-earth dopants on phase structure and electrical properties of lead-free bismuth sodium titanate-based ceramics, *Journal of Materiomics*. 6 (2020) 286–292. <https://doi.org/10.1016/j.jmat.2020.03.005>.
- [51] F. Li, D. Lin, Z. Chen, Z. Cheng, J. Wang, C. Li, Z. Xu, Q. Huang, X. Liao, L.-Q. Chen, T.R. Shrout, S. Zhang, Ultrahigh piezoelectricity in ferroelectric ceramics by design, *Nature Materials*. 17 (2018) 349–354. <https://doi.org/10.1038/s41563-018-0034-4>.
- [52] A. Lahmar, S. Habouti, C.-H. Solterbeck, M. Es-Souni, B. Elouadi, Correlation between structure, dielectric, and ferroelectric properties in $\text{BiFeO}_3\text{--LaMnO}_3$ solid solution thin films, *Journal of Applied Physics*. 105 (2009) 014111. <https://doi.org/10.1063/1.3063813>.
- [53] M. Zannen, H. Khemakhem, A. Kabadou, M. Es-Souni, Structural, Raman and electrical studies of 2at.% Dy-doped NBT, *Journal of Alloys and Compounds*. 555 (2013) 56–61. <https://doi.org/10.1016/j.jallcom.2012.12.002>.
- [54] R. Roukos, N. Zaiter, D. Chaumont, Relaxor behaviour and phase transition of perovskite ferroelectrics-type complex oxides $(1-x)\text{Na}_0.5\text{Bi}_0.5\text{TiO}_3-x\text{CaTiO}_3$ system, *J Adv Ceram*. 7 (2018) 124–142. <https://doi.org/10.1007/s40145-018-0264-6>.
- [55] E. Aksel, J.S. Forrester, B. Kowalski, M. Deluca, D. Damjanovic, J.L. Jones, Structure and properties of Fe-modified $\text{Na}_0.5\text{Bi}_0.5\text{TiO}_3$ at ambient and elevated temperature, *Physical Review B*. 85 (2012) 024121. <https://doi.org/10.1103/PhysRevB.85.024121>.
- [56] S. Saïd, P. Marchet, T. Merle-Méjean, J.-P. Mercurio, Raman spectroscopy study of the $\text{Na}_0.5\text{Bi}_0.5\text{TiO}_3\text{--PbTiO}_3$ system, *Materials Letters*. 58 (2004) 1405–1409. <https://doi.org/10.1016/j.matlet.2003.09.036>.
- [57] K. Thangavelu, S. Asthana, MonoclinicCc-phase stabilization in magnetically diluted lead free $\text{Na}_{1/2}\text{Bi}_{1/2}\text{TiO}_3$ —Evolution of spin glass like behavior with enhanced ferroelectric and dielectric properties, *Mater. Res. Express*. 2 (2015) 096301. <https://doi.org/10.1088/2053-1591/2/9/096301>.

- [58] B.K. Barick, K.K. Mishra, A.K. Arora, R.N.P. Choudhary, D.K. Pradhan, Impedance and Raman spectroscopic studies of $(\text{Na}_{0.5}\text{Bi}_{0.5})\text{TiO}_3$, *J. Phys. D: Appl. Phys.* 44 (2011) 355402. <https://doi.org/10.1088/0022-3727/44/35/355402>.
- [59] J. Kreisel, A.M. Glazer, G. Jones, P.A. Thomas, L. Abello, G. Lucazeau, An x-ray diffraction and Raman spectroscopy investigation of A-site substituted perovskite compounds: the $(\text{Na}_{1-x}\text{K}_x)\text{Bi}_{0.5}\text{TiO}_3$ ($0 \leq x \leq 1$) solid solution, *Journal of Physics Condensed Matter*. 12 (2000) 3267–3280. <https://doi.org/10.1088/0953-8984/12/14/305>.
- [60] G. Trolliard, V. Dorcet, Reinvestigation of Phase Transitions in $\text{Na}_{0.5}\text{Bi}_{0.5}\text{TiO}_3$ by TEM. Part II: Second Order Orthorhombic to Tetragonal Phase Transition, *Chemistry of Materials*. 20 (2008) 5074–5082. <https://doi.org/10.1021/cm800464d>.
- [61] V. Dorcet, G. Trolliard, P. Boullay, Reinvestigation of Phase Transitions in $\text{Na}_{0.5}\text{Bi}_{0.5}\text{TiO}_3$ by TEM. Part I: First Order Rhombohedral to Orthorhombic Phase Transition, *Chem. Mater.* 20 (2008) 5061–5073. <https://doi.org/10.1021/cm8004634>.
- [62] G. Wang, Z. Lu, Z. Zhang, A. Feteira, C.C. Tang, D.A. Hall, Electric field-induced irreversible relaxor to ferroelectric phase transformations in $\text{Na}_{0.5}\text{Bi}_{0.5}\text{TiO}_3\text{-NaNbO}_3$ ceramics, *Journal of the American Ceramic Society*. 102 (2019) 7746–7754. <https://doi.org/10.1111/jace.16676>.
- [63] S. Murakami, D. Wang, A. Mostaed, A. Khesro, A. Feteira, D.C. Sinclair, Z. Fan, X. Tan, I.M. Reaney, High strain (0.4%) $\text{Bi}(\text{Mg}_{2/3}\text{Nb}_{1/3})\text{O}_3\text{-BaTiO}_3\text{-BiFeO}_3$ lead-free piezoelectric ceramics and multilayers, *Journal of the American Ceramic Society*. 101 (2018) 5428–5442. <https://doi.org/10.1111/jace.15749>.
- [64] D. Wang, Z. Fan, W. Li, D. Zhou, A. Feteira, G. Wang, S. Murakami, S. Sun, Q. Zhao, X. Tan, I.M. Reaney, High Energy Storage Density and Large Strain in $\text{Bi}(\text{Zn}_{2/3}\text{Nb}_{1/3})\text{O}_3\text{-Doped BiFeO}_3\text{-BaTiO}_3$ Ceramics, *ACS Appl. Energy Mater.* 1 (2018) 4403–4412. <https://doi.org/10.1021/acsaem.8b01099>.
- [65] C. Zhou, Q. Li, J. Xu, L. Yang, W. Zeng, C. Yuan, G. Chen, Ferroelectric-quasiferroelectric-ergodic relaxor transition and multifunctional electrical properties in $\text{Bi}_{0.5}\text{Na}_{0.5}\text{TiO}_3$ -based ceramics, *Journal of the American Ceramic Society*. 101 (2018) 1554–1565. <https://doi.org/10.1111/jace.15308>.
- [66] A. Zeb, S.J. Milne, High temperature dielectric ceramics: a review of temperature-stable high-permittivity perovskites, *J Mater Sci: Mater Electron*. 26 (2015) 9243–9255. <https://doi.org/10.1007/s10854-015-3707-7>.
- [67] L. Yang, X. Kong, F. Li, H. Hao, Z. Cheng, H. Liu, J.-F. Li, S. Zhang, Perovskite lead-free dielectrics for energy storage applications, *Progress in Materials Science*. 102 (2019) 72–108. <https://doi.org/10.1016/j.pmatsci.2018.12.005>.
- [68] B. Fan, F. Liu, G. Yang, H. Li, G. Zhang, S. Jiang, Q. Wang, Dielectric materials for high-temperature capacitors, *IET Nanodielectrics*. 1 (2018) 32–40. <https://doi.org/10.1049/iet-nde.2018.0002>.
- [69] M. Benyoussef, M. Zannen, J. Belhadi, B. Manoun, J.-L. Dellis, M. El Marssi, A. Lahmar, Dielectric, ferroelectric, and energy storage properties in dysprosium doped sodium bismuth titanate ceramics, *Ceramics International*. 44 (2018) 19451–19460. <https://doi.org/10.1016/j.ceramint.2018.07.182>.
- [70] K. Bridger, A.V. Cooke, W.A. Schulze, High-temperature dielectric materials and capacitors made therefrom, US7697263B2, 2010. <https://patents.google.com/patent/US7697263B2/en> (accessed May 10, 2020).
- [71] R. Dittmer, W. Jo, D. Damjanovic, J. Rödel, Lead-free high-temperature dielectrics with wide operational range, *Journal of Applied Physics*. 109 (2011) 034107. <https://doi.org/10.1063/1.3544481>.
- [72] CARTS international 2013: Houston, Texas, USA, 25-28 March 2013., 2013.
- [73] G. Wang, D.A. Hall, Y. Li, C.A. Murray, C.C. Tang, Structural characterization of the electric field-induced ferroelectric phase in $\text{Na}_{0.5}\text{Bi}_{0.5}\text{TiO}_3\text{-KNbO}_3$ ceramics, *Journal of the European Ceramic Society*. 36 (2016) 4015–4021. <https://doi.org/10.1016/j.jeurceramsoc.2016.06.022>.

- [74] H. Guo, X. Liu, F. Xue, L.-Q. Chen, W. Hong, X. Tan, Disrupting long-range polar order with an electric field, *Phys. Rev. B.* 93 (2016) 174114. <https://doi.org/10.1103/PhysRevB.93.174114>.
- [75] G. Viola, H. Ning, X. Wei, M. Deluca, A. Adomkevicius, J. Khaliq, M. John Reece, H. Yan, Dielectric relaxation, lattice dynamics and polarization mechanisms in Bi_{0.5}Na_{0.5}TiO₃-based lead-free ceramics, *Journal of Applied Physics.* 114 (2013) 014107. <https://doi.org/10.1063/1.4812383>.
- [76] F. Li, G. Chen, X. Liu, J. Zhai, B. Shen, S. Li, P. Li, K. Yang, H. Zeng, H. Yan, Type-I pseudo-first-order phase transition induced electrocaloric effect in lead-free Bi_{0.5}Na_{0.5}TiO₃-0.06BaTiO₃ ceramics, *Appl. Phys. Lett.* 110 (2017) 182904. <https://doi.org/10.1063/1.4983029>.
- [77] X. Yan, M. Zhu, Q. Wei, S.-G. Lu, M. Zheng, Y. Hou, Large electrocaloric effect in tetragonal perovskite 0.03Bi(Mg_{1/2}Ti_{1/2})O₃-0.97(0.875Bi_{1/2}Na_{1/2}TiO₃-0.125BaTiO₃) lead-free ferroelectric ceramics, *Scripta Materialia.* 162 (2019) 256-260. <https://doi.org/10.1016/j.scriptamat.2018.11.007>.
- [78] E.-M. Anton, W. Jo, D. Damjanovic, J. Rödel, Determination of depolarization temperature of (Bi_{1/2}Na_{1/2})TiO₃-based lead-free piezoceramics, *Journal of Applied Physics.* 110 (2011) 094108. <https://doi.org/10.1063/1.3660253>.
- [79] F. Li, G. Chen, X. Liu, J. Zhai, B. Shen, H. Zeng, S. Li, P. Li, K. Yang, H. Yan, Phase-composition and temperature dependence of electrocaloric effect in lead-free Bi_{0.5}Na_{0.5}TiO₃-BaTiO₃-(Sr_{0.7}Bi_{0.2}□_{0.1})TiO₃ ceramics, *Journal of the European Ceramic Society.* 37 (2017) 4732-4740. <https://doi.org/10.1016/j.jeurceramsoc.2017.06.033>.
- [80] A.A. Bokov, Z.-G. Ye, Recent progress in relaxor ferroelectrics with perovskite structure, *J Mater Sci.* 41 (2006) 31-52. <https://doi.org/10.1007/s10853-005-5915-7>.
- [81] G. Zhang, M. Chen, B. Fan, Y. Liu, M. Li, S. Jiang, H. Huang, H. Liu, H. Li, Q. Wang, High electrocaloric effect in hot-pressed Pb_{0.85}La_{0.1}(Zr_{0.65}Ti_{0.35})O₃ ceramics with a wide operating temperature range, *Journal of the American Ceramic Society.* 100 (2017) 4581-4589. <https://doi.org/10.1111/jace.14984>.
- [82] Q. Li, M. Li, C. Wang, M. Zhang, H. Fan, Enhanced temperature stable dielectric properties and energy-storage density of BaSnO₃-modified (Bi_{0.5}Na_{0.5})_{0.94}Ba_{0.06}TiO₃ lead-free ceramics, *Ceramics International.* 45 (2019) 19822-19828. <https://doi.org/10.1016/j.ceramint.2019.06.237>.
- [83] Z. Liu, P. Ren, C. Long, X. Wang, Y. Wan, G. Zhao, Enhanced energy storage properties of NaNbO₃ and SrZrO₃ modified Bi_{0.5}Na_{0.5}TiO₃ based ceramics, *Journal of Alloys and Compounds.* 721 (2017) 538-544. <https://doi.org/10.1016/j.jallcom.2017.05.162>.
- [84] Q. Xu, M.T. Lanagan, X. Huang, J. Xie, L. Zhang, H. Hao, H. Liu, Dielectric behavior and impedance spectroscopy in lead-free BNT-BT-NBN perovskite ceramics for energy storage, *Ceramics International.* 42 (2016) 9728-9736. <https://doi.org/10.1016/j.ceramint.2016.03.062>.
- [85] W. Cao, W. Li, T. Zhang, J. Sheng, Y. Hou, Y. Feng, Y. Yu, W. Fei, High-Energy Storage Density and Efficiency of (1-x)[0.94 NBT-0.06 BT]-xST Lead-Free Ceramics, *Energy Technology.* 3 (2015) 1198-1204. <https://doi.org/10.1002/ente.201500173>.
- [86] F. Li, J. Zhai, B. Shen, X. Liu, K. Yang, Y. Zhang, P. Li, B. Liu, H. Zeng, Influence of structural evolution on energy storage properties in Bi_{0.5}Na_{0.5}TiO₃-SrTiO₃-NaNbO₃ lead-free ferroelectric ceramics, *Journal of Applied Physics.* 121 (2017) 054103. <https://doi.org/10.1063/1.4975409>.
- [87] X. Wang, H. Gao, X. Hao, X. Lou, Enhanced piezoelectric, electrocaloric and energy storage properties at high temperature in lead-free Bi_{0.5}(Na_{1-x}K_x)_{0.5}TiO₃ ceramics, *Ceramics International.* 45 (2019) 4274-4282. <https://doi.org/10.1016/j.ceramint.2018.11.100>.
- [88] R.A. Malik, A. Hussain, A. Maqbool, A. Zaman, T.K. Song, W.-J. Kim, M.-H. Kim, Giant strain, thermally-stable high energy storage properties and structural evolution of Bi-based lead-free piezoceramics, *Journal of Alloys and Compounds.* 682 (2016) 302-310. <https://doi.org/10.1016/j.jallcom.2016.04.297>.
- [89] B. Hu, H. Fan, L. Ning, S. Gao, Z. Yao, Q. Li, Enhanced energy-storage performance and dielectric temperature stability of (1-x)(0.65Bi_{0.5}Na_{0.5}TiO₃-0.35Bi_{0.1}Sr_{0.85}TiO₃)-xKNbO₃ ceramics,

- Ceramics International. 44 (2018) 10968–10974.
<https://doi.org/10.1016/j.ceramint.2018.03.176>.
- [90] L. Zhang, Y. Pu, M. Chen, T. Wei, X. Peng, Novel Na_{0.5}Bi_{0.5}TiO₃ based, lead-free energy storage ceramics with high power and energy density and excellent high-temperature stability, *Chemical Engineering Journal*. 383 (2020) 123154. <https://doi.org/10.1016/j.cej.2019.123154>.
- [91] B. Yan, H. Fan, A.K. Yadav, C. Wang, X. Zheng, H. Wang, W. Wang, W. Dong, S. Wang, Enhanced energy-storage performance and thermally stable permittivity for K_{0.5}Na_{0.5}NbO₃ modified [(Na_{0.5}Bi_{0.5})_{0.84}Sr_{0.16}]_{0.98}La_{0.01}TiO₃ lead-free perovskite ceramics, *Ceramics International*. 46 (2020) 9637–9645. <https://doi.org/10.1016/j.ceramint.2019.12.230>.
- [92] B. Rožič, M. Kosec, H. Uršič, J. Holc, B. Malič, Q.M. Zhang, R. Blinc, R. Pirc, Z. Kutnjak, Influence of the critical point on the electrocaloric response of relaxor ferroelectrics, *Journal of Applied Physics*. 110 (2011) 064118. <https://doi.org/10.1063/1.3641975>.
- [93] P.-Z. Ge, X.-G. Tang, Q.-X. Liu, Y.-P. Jiang, W.-H. Li, J. Luo, Energy storage properties and electrocaloric effect of Ba_{0.65}Sr_{0.35}TiO₃ ceramics near room temperature, *J Mater Sci: Mater Electron*. 29 (2018) 1075–1081. <https://doi.org/10.1007/s10854-017-8008-x>.
- [94] P.-Z. Ge, X.-D. Jian, X.-W. Lin, X.-G. Tang, Z. Zhu, Q.-X. Liu, Y.-P. Jiang, T.-F. Zhang, S.-G. Lu, Composition dependence of giant electrocaloric effect in PbxSr_{1-x}TiO₃ ceramics for energy-related applications, *Journal of Materiomics*. 5 (2019) 118–126. <https://doi.org/10.1016/j.jmat.2018.10.002>.
- [95] J. Li, J. Li, S. Qin, X. Su, L. Qiao, Y. Wang, T. Lookman, Y. Bai, Effects of Long- and Short-Range Ferroelectric Order on the Electrocaloric Effect in Relaxor Ferroelectric Ceramics, *Phys. Rev. Applied*. 11 (2019) 044032. <https://doi.org/10.1103/PhysRevApplied.11.044032>.
- [96] F. Li, J. Li, J. Zhai, B. Shen, S. Li, M. Zhou, K. Zhao, H. Zeng, Influence of structural evolution on electrocaloric effect in Bi_{0.5}Na_{0.5}TiO₃-SrTiO₃ ferroelectric ceramics, *Journal of Applied Physics*. 124 (2018) 164108. <https://doi.org/10.1063/1.5050826>.
- [97] A.-K. Axelsson, F. Le Goupil, M. Valant, N.McN. Alford, Optimisation of SrBi₂(Nb,Ta)₂O₉ Aurivillius phase for lead-free electrocaloric cooling, *Journal of the European Ceramic Society*. 38 (2018) 5354–5358. <https://doi.org/10.1016/j.jeurceramsoc.2018.07.044>.
- [98] K.R. Kandula, K. Banerjee, S.S.K. Raavi, S. Asthana, Enhanced Electrocaloric Effect and Energy Storage Density of Nd-Substituted 0.92NBT-0.08BT Lead Free Ceramic, *Physica Status Solidi (a)*. 215 (2018) 1700915. <https://doi.org/10.1002/pssa.201700915>.
- [99] F. Le Goupil, J. Bennett, A.-K. Axelsson, M. Valant, A. Berenov, A.J. Bell, T.P. Comyn, N.McN. Alford, Electrocaloric enhancement near the morphotropic phase boundary in lead-free NBT-KBT ceramics, *Appl. Phys. Lett*. 107 (2015) 172903. <https://doi.org/10.1063/1.4934759>.
- [100] J. Yang, Y. Zhao, X. Lou, J. Wu, X. Hao, Synergistically optimizing electrocaloric effects and temperature span in KNN-based ceramics utilizing a relaxor multiphase boundary, *Journal of Materials Chemistry C*. 8 (2020) 4030–4039. <https://doi.org/10.1039/C9TC06443E>.
- [101] X. Jiang, L. Luo, B. Wang, W. Li, H. Chen, Electrocaloric effect based on the depolarization transition in (1-x)Bi_{0.5}Na_{0.5}TiO₃-xKNbO₃ lead-free ceramics, *Ceramics International*. 40 (2014) 2627–2634. <https://doi.org/10.1016/j.ceramint.2013.10.066>.
- [102] W.P. Cao, W.L. Li, D. Xu, Y.F. Hou, W. Wang, W.D. Fei, Enhanced electrocaloric effect in lead-free NBT-based ceramics, *Ceramics International*. 40 (2014) 9273–9278. <https://doi.org/10.1016/j.ceramint.2014.01.149>.
- [103] F. Le Goupil, A. Baker, F. Tonus, A. Berenov, C.A. Randall, N.McN. Alford, Direct measurement of electrocaloric effect in lead-free (Na_{0.5}Bi_{0.5})TiO₃-based multilayer ceramic capacitors, *Journal of the European Ceramic Society*. 39 (2019) 3315–3319. <https://doi.org/10.1016/j.jeurceramsoc.2019.04.032>.
- [104] F. Le Goupil, R. McKinnon, V. Koval, G. Viola, S. Dunn, A. Berenov, H. Yan, N.M. Alford, Tuning the electrocaloric enhancement near the morphotropic phase boundary in lead-free ceramics, *Scientific Reports*. 6 (2016) 28251. <https://doi.org/10.1038/srep28251>.